Thus, our rat models of autism are well suited for investigations of the embryonic development of the nervous system.

Although the embryonic development of facial nerves in our rat model of autism has not been fully characterized, embryonic VPA treatment has been shown to reduce the number of adult motor neurons, including those of the facial nuclei (Rodier et al., 1996), resulting in anatomical anomalies within the cranial motor nuclei. Moreover, we previously reported on morphological abnormalities in the peripheral facial nerves in an embryonic rat model of autism (Tashiro et al., 2011). In these rats, peripheral facial nerves became truncated and defasciculated (Tashiro et al., 2011). In addition, Ornoy (2009) reviewed the relationship between VPA and autism, including experiments using VPA to generate animal models of autism, and concluded that experimental animal models generally mimic the effects of VPA in man, although animals seem to be more resistant to VPA than humans. Taken together, these findings suggest that the development of facial neurons, not only in the peripheral nerves but also in the central hindbrain, including the facial nuclei, should be examined after VPA exposure.

In the present study, to examine the caudal migration of neurons and the initial formation of facial nuclei in a rat model of autism, VPA was administered to pregnant rats at E9.5. This enables delivery to the embryos *via* the placenta and subsequent distribution to the facial nuclei. We utilized a combination of flat whole-mount preparations and *in situ* hybridization for molecular markers expressed in the cranial motor neurons to allow us to clearly identify the facial nuclei and quantify their size for statistical analysis.

2. Material and methods

2.1. Animals and teratogen exposure

All experiments involving animals were approved by the Community of Laboratory Animal Research Center at the University of Mie, Japan. Details of the teratogen administration have been previously described (Miyazaki et al., 2005; Narita Naoko et al., 2002; Narita Masaaki et al., 2010). In brief, female Wistar rats (2–6 months old) were mated overnight and the day of insemination was designated as embryonic day (E) 0.5. On E9.5, at 1:00 p.m., 800 mg/kg VPA was administered orally without sedation to dams in each group using an infant feeding tube (Atom Medical, Tokyo, Japan) attached to a 2.5 ml disposable syringe. We referred to prior animal experiments using these teratogens to determine the doses of VPA (Ingram et al., 2000). Because our previous study showed that VPA exposure after E9.5 induced morphological abnormalities of facial nerves (Tashiro et al., 2011), we adopted E9.5 as the day of administration. VPA was prepared by dissolving the drug in 5% arabic gum in distilled water. No pregnant mothers died from the dose of VPA, and most embryos survived.

2.2. Flat whole-mount preparations of rat hindbrain

Embryos were removed from the dams at E13.5, E14.5 or E15.5, and the crown–rump length (CRL) was measured at each stage. The portion of the head containing the midbrain and hindbrain was dissected out in cold phosphate-buffered saline (PBS). To obtain flat whole-mount preparations of the hindbrain, the dorsal midline of the neural tube was completely cut and the 4th ventricle was opened. The isthmus of the midbrain–hindbrain boundary was cut, and the hindbrain was carefully freed from the meninges and surrounding tissue while keeping the trigeminal ganglion and vestibular ganglion, as well as their roots, intact.

Flat whole-mounted hindbrains were fixed in 4% paraformaldehyde in PBS for 7–10 h at 4 °C. Tissues were then washed twice with Tris-buffered saline (TBS), dehydrated through a graded methanol/TBS series at 4 °C, and stored in 100% methanol at −20 °C.

In observing tissues under a microscope, to ensure equal pressure across whole-mounted hindbrains, multiple layers of plastic tape were inserted as supports between the slide and coverslip. Because the layered plastic tape supports the load from the coverslip, the preparations received equal pressure in all locations and were not transformed by unequal pressure.

2.3. In situ hybridization

A DNA fragment corresponding to a portion of rat *Tbx20* (nucleotides 51–885, GenBank NM_001108132) or *cdh8* (nucleotides 1909–2435, GenBank NM_053393.2) cDNA was cloned into the pGEM-T Easy vector (Promega, La Jolla, CA). Using this plasmid as a template, sense and antisense single-strand RNA probes were synthesized using a digoxigenin labeling kit (Roche Diagnostics, Tokyo, Japan). Whole-mount *in situ* hybridization using sense probes detected no signal except background noise, demonstrating specific hybridization to the target sequences.

In situ hybridization on flat whole-mounted hindbrains was performed according to the methods of Nieto et al. (1996), with minor modifications. Tissues were treated with 0.3% H_2O_2/methanol for 30 min and rehydrated through a graded methanol/PBST series. The hindbrains were then treated with 10 μg/ml proteinase K/PBST and fixed in 0.2% glutaraldehyde/4% paraformaldehyde in PBS. After rinsing three times for 5 min in PBST, they were prehybridized in prehybridization solution (50% formamide; 5 × SSC; 50 μg/ml yeast RNA (Roche); 50 μg/ml heparin (Roche); 5 mM EDTA; 1% SDS). Tissue was then incubated in hybridization solution (prehybridization solution containing 1 mg/ml probe) overnight at 60 C. After high-stringency washes, the tissues were blocked for 2 h in blocking reagent (Roche) and incubated in a 1/500 dilution of anti-digoxigenin-AP conjugate (Roche) in blocking reagent for 3 h. After an overnight wash with TBST, the signals were visualized in NTMT (0.1 M Tris–HCl, 0.1 M NaCl, 0.05 M $MgCl_2$, and 0.1% Tween 20) containing nitroblue tetrazolium chloride/5-bromo-4-chloro-3-indolyl phosphate, toluidine salt (Roche).

2.4. Statistical analysis

Embryos from at least three different dams were analyzed for each condition. Bilateral facial nuclei were analyzed in each embryo and the number of analyzed facial nuclei pairs is referred to in the text as "n=". Digital images were captured using a light microscope equipped with a CCD camera (DXM1200F, Nikon, Tokyo, Japan). The intensities of *Tbx20* or *cdh8* signals and the sizes of the areas circumscribed by these signals were measured using Image J software. Signal intensity was defined such that complete white was scored as "0" and complete black as "255". The relative level of signal intensity was determined by comparison with the signal intensity in the control group. The boundaries of these regions were determined based on the signal threshold, excluding background noise. The mean and standard deviation (SD) was calculated, and differences among developmental stages were evaluated using *t*-tests.

3. Results

3.1. Development of Tbx20-positive facial motor neurons

To elucidate the development of the cranial motor nuclei within the hindbrain, in relation to the rostrocaudal and dorsoventral axes, flat whole-mount preparations (Fig. 1) from E13.5, 14.5 and 15.5 embryos were analyzed. Flat whole-mount embryonic hindbrain preparations were subjected to *in situ* hybridization using an RNA probe for *Tbx20*, which is expressed in early cranial motor neurons (Figs. 2 and 3).

In whole-mount preparations from control embryos at E13.5, intense *Tbx20* signals were observed near the floor plate between the vestibular ganglia, corresponding to r4 at the rostrocaudal level (Fig. 2A). Weak *Tbx20* signals were observed in the ventral column lateral to the floor plate (data not shown). In whole-mount preparations from embryos exposed to VPA *in utero*, the pattern of *Tbx20* expression was similar (Fig. 2B).

At E14.5 in the control group, *Tbx20* signals extended from r4 through r5–6 in a caudolateral direction (Fig. 2C, arrows). Toward the caudal end of the *Tbx20* expression domain, the signal faded out (Fig. 2C, arrowheads). These signal patterns were similar to those observed in the VPA-exposed group (Fig. 2D).

Because flat whole-mount preparations are much thicker at E15.5 than they are at earlier stages, *Tbx20* signals could be observed more clearly from either the ventricular or pial sides (Fig. 3). In the control group, despite limited *Tbx20* expression near the floor plate on the ventricular side (Fig. 3A, arrows), the caudal end of the *Tbx20* signals was located on the pial side and had an ovoid appearance (Fig. 3C, asterisks). In addition, intense *Tbx20* signals were also observed between the trigeminal ganglia, corresponding to r2 at the rostrocaudal level on the pial side (Fig. 3C and D, arrowheads).

In the VPA-exposed group, the pattern of *Tbx20* expression was similar (Fig. 3B and D). However, the signals near the floor plate were more intense than those in the control

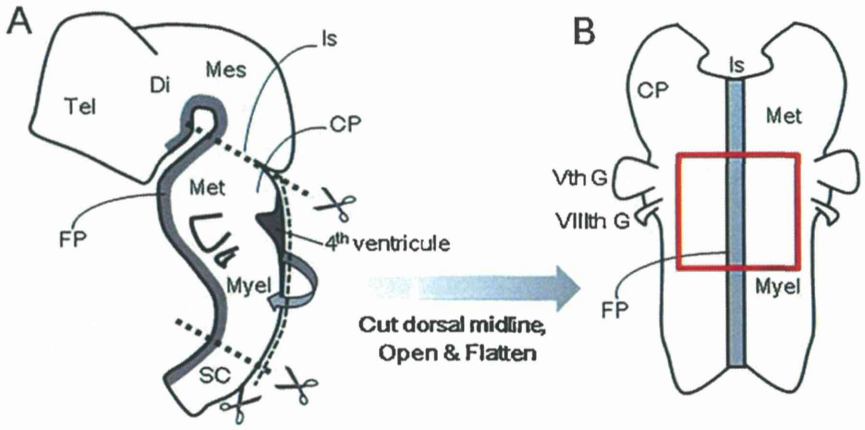

Fig. 1. Flat whole-mount preparation of the hindbrain. (A) Schematic diagram showing the cut site in the neural tube. Embryonic rat hindbrains were dissected and oriented with the ventricular side down (Tashiro et al., 2000). (B) Schematic diagram of a flat whole-mount preparation of the hindbrain. Figs. 2, 3 and 5 correspond to the area outlined by the red square in B. CP: cerebellar plate, Di: diencephalon, FP: floor plate, Is: isthmus, Mes: mesencephalon, Met: metencephalon, Myel: myelencephalon, Tel: telencephalon, SC: spinal cord, Vth G: trigeminal ganglion, VIIIth G: vestibular ganglion. (For interpretation of the references to color in this figure legend, the reader is referred to the web version of the article).

group (Fig. 3B, arrows) and the oval *Tbx20*-positive region appeared to be smaller than it was in controls (Fig. 3C and D, asterisks). The pattern of *Tbx20* signals near the floor plate was considered to represent the migratory pathway of facial motor neurons, and the oval areas positive for *Tbx20* signals at the caudal end were considered to represent the facial nuclei.

To identify differences in the migratory pathways and the sizes of facial nuclei between control and VPA-exposed groups, the *Tbx20*-positive areas were measured. The area of the *Tbx20*-positive migratory pathway ($\times 10^4\ \mu m^2$) was 0.66 ± 0.17 in the control group ($n = 6$) and 1.37 ± 0.31 in the VPA-exposed group ($n = 12$), revealing a significant increase in the size of the pathway in embryos exposed to VPA compared with controls ($p < 0.001$). The area of the *Tbx20*-positive facial nuclei ($\times 10^4\ \mu m^2$) was 9.33 ± 0.92 in the control group ($n = 6$) and 7.55 ± 1.02 in the VPA-exposed group ($n = 12$), revealing a significant reduction in the size of these nuclei compared with controls ($p < 0.01$). When the sizes of *Tbx20*-positive facial nuclei were plotted against the sizes of *Tbx20*-positive migratory pathways (Fig. 4), the resulting graph showed an inverse relationship between the two, with increasing size of the migratory pathway and

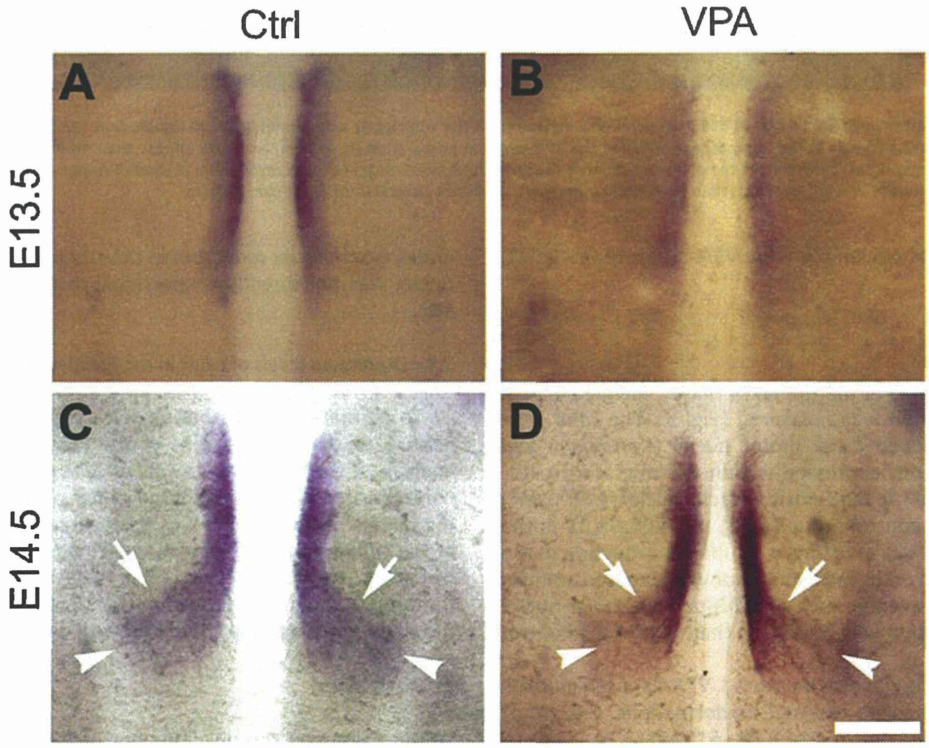

Fig. 2. *Tbx20* expression patterns at E13.5 and E14.5. (A and B) E13.5 preparations showing *Tbx20* signals near the floor plate in the control group (A) and VPA-exposed group (B). (C and D) E14.5 preparations showing *Tbx20* signals near the floor plate in the control group (C) and VPA-exposed group (D). *Tbx20* signals extend in a caudolateral direction (arrows). Near the caudal end of the *Tbx20* expression domain, the signal fades out (arrowheads). Rostral is up. Scale bar: 250 μm.

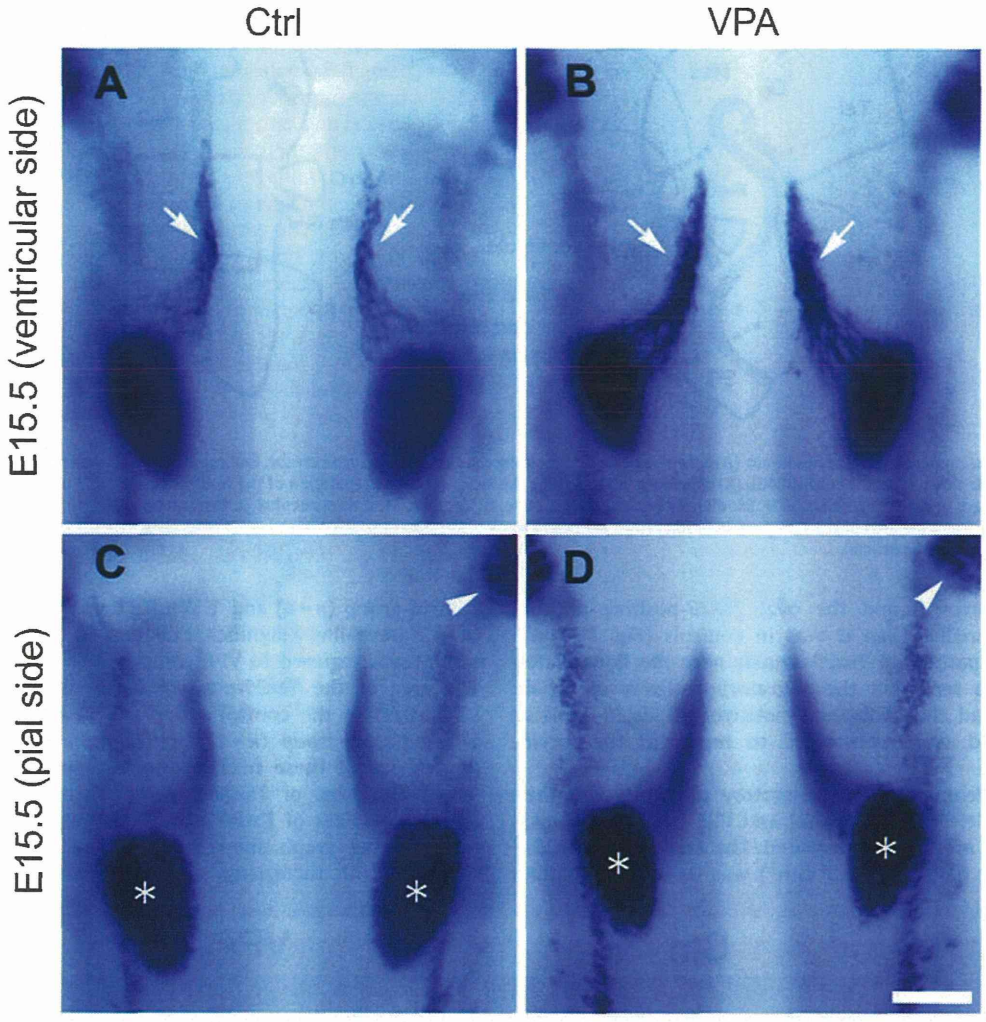

Fig. 3. *Tbx20* expression pattern at E15.5. (A and B) E15.5 preparations, viewed from the ventricular side, showing *Tbx20* signals near the floor plate in the control group (A) and VPA-exposed group (B). Signals in the migratory pathway of the VPA-exposed preparation (B, arrows) are more intense than those in the control preparation (A, arrows). (C and D) E15.5 preparations, viewed from the pial side, showing *Tbx20*-positive facial nuclei in the control group (C) and VPA-exposed group (D). The facial nuclei are smaller in embryos exposed to VPA (D, asterisks) than in control embryos (C, asterisks). Rostral is up. Scale bar: 250 μm.

decreasing size of facial nuclei following VPA exposure ($p < 0.001$; $R = -0.74$).

3.2. Size of facial nuclei

To determine the sizes of mature facial nuclei, the area of *cadherin 8* (*cdh8*) expression was measured (Fig. 5). The *cdh8* gene is expressed in developed facial motor nuclei (Korematsu and Redies, 1997), and is not expressed within the migratory pathway (Fig. 5). The area of the *cdh8*-positive facial nuclei ($\times 10^4$ μm^2) was 9.87 ± 0.43 in the control group ($n = 4$) and 7.06 ± 1.31 in the VPA-exposed group ($n = 5$), revealing a significant reduction in the area of *cdh8* expression in the facial nuclei of VPA-exposed animals ($p < 0.01$). Indeed, the average area of *cdh8*-positive facial nuclei in the VPA-exposed group was 28.4% less than that in the control group.

CRL of E15.5 embryos was also measured. VPA-exposed animals appeared robust and had no external malformations. CRL (mm) was 12.80 ± 0.37 in the control group ($n = 5$) and 12.24 ± 0.18 in the VPA-exposed group ($n = 4$), revealing a significant reduction in CRL in VPA-exposed embryos at E15.5 ($p < 0.05$). The average CRL in VPA-exposed embryos was only 4.3% less than that in control embryos; thus, the reduction in the size of the *cdh8*-positive facial nuclei was not directly proportional to the reduction in average CRL.

3.3. Expression levels of cdh8 in the facial nuclei

To estimate the contribution of the cell adhesion molecule *cadherin 8* to the development of the facial nuclei, a preliminary analysis of the expression levels of *cdh8* was performed. The signal intensity in the VPA-exposed group was normalized to that in the control group, which was designated as 100%. The intensity of the *cdh8* signal in the facial nuclei was 100.0 ± 2.8 in the control group ($n = 4$) and 84.5 ± 12.2 in the VPA-exposed group ($n = 5$), revealing a significant reduction (by 15.5%) in *cdh8* expression in the VPA-exposed group compared with controls ($p < 0.05$).

4. Discussion

We examined the development of facial nuclei in an animal model of autism, established by *in utero* exposure to VPA, using *in situ* hybridization for the molecular markers *Tbx20* and *cdh8*. Analysis of *Tbx20* expression revealed similar patterns of caudal

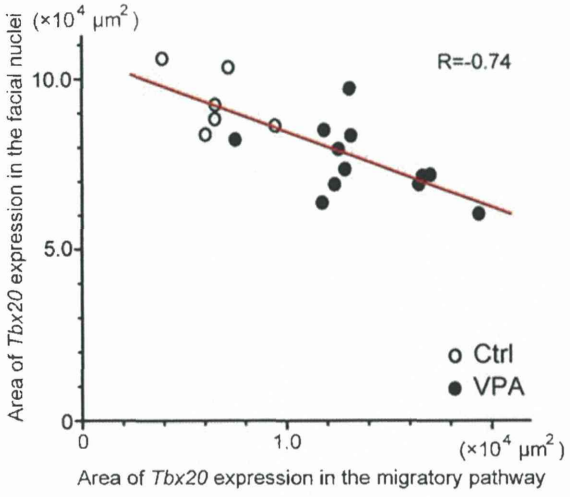

Fig. 4. Correlation between the area of the *Tbx20*-positive migratory pathway and the facial nucleus. The increase in the size of the migratory pathway is inversely proportional to the reduction in the size of the facial nucleus ($p < 0.001$, $R = -0.74$). Open circles: control group, filled circles: VPA-exposed group.

migration of neurons to the facial nuclei in control and VPA-exposed groups; however, this caudal migration of neurons was hindered in animals exposed to VPA, with the result that the facial nuclei were significantly smaller in these animals. Our data provide the first description of tangential migration and nucleus formation in the developing hindbrain in a rat model of autism. Moreover, this disruption during early development of the facial nuclei might contribute to the etiology of autism with facial palsy.

4.1. Technical consideration

To assess the distribution of *Tbx20* and *cdh8* signals in the developing hindbrain, flat whole-mount preparations (Tashiro et al., 2000, 2007) were used. These allowed us to observe signal distributions within both the rostrocaudal and dorsoventral axes, without requiring the reconstruction of serial sections. Because later-stage whole-mount preparations are not suitable for an analysis of signal depth, we restricted our observations to the ventricular and pial sides at E15.5.

Facial nuclei were identified based on the expression of *Tbx20* and *cdh8* mRNA signals and their anatomical locations within the flat whole-mount preparations. Because *Tbx20* is expressed in all early-stage cranial motor neurons (Kraus et al., 2001; Meins et al., 2000; Song et al., 2006), it was not possible to distinguish the facial nuclei from the abducens or trigeminal motor nuclei. However, using flat whole-mount preparations enabled us to positively identify the migratory pathways taken by neurons to reach these nuclei based on anatomical landmarks as well as the positioning of the ganglia and their roots. The trigeminal ganglion is positioned near rostrocaudal level r2, and *Tbx20* signals near the trigeminal ganglion are considered to represent the trigeminal motor nuclei (Noden, 1993). The vestibular ganglion is positioned near rostrocaudal level r4; *Tbx20* signals near the floor plate between these ganglia are considered to represent the facial motor nuclei. The neurons that comprise the facial nuclei originate in r4 and migrate caudally to r6; their migratory pathways are well-described in the literature (Chandrasekhar, 2004; Hatten, 1999; Noden, 1993; Yamamoto and Schwarting, 1991) and are consistent with the signal patterns we observed. The expansion of the area of *Tbx20*-positive signals is likely correlated to the migration of neurons to and shape of facial motor nuclei. Thus, the combination of *Tbx20* signals and positional information in flat whole-mount preparations is an appropriate tool for evaluating the development of facial nuclei.

In addition to *Tbx20* signals, *cdh8* signals can be used to visualize mature facial nuclei (Korematsu and Redies, 1997). Because *cdh8* is not expressed in the migratory pathways of neurons destined for the facial nuclei or other cranial motor nuclei in the hindbrain, *cdh8* signals enable us to specifically identify the area of the facial nuclei. Quantification of facial nucleus area based on *cdh8* expression is therefore more precise than measurements based on *Tbx20* expression. We have provided the first numerical quantification of the area of the developing facial nuclei following exposure to VPA *in utero*.

4.2. Development of the facial nuclei in a rat model of autism

The caudal migration patterns of neurons destined for the facial nuclei in a rat model of autism induced by VPA exposure were similar to those seen in normal control rats. However, VPA exposure hindered this migration and significantly reduced the area of the facial nuclei. Although CRL was also reduced in the VPA-exposed group, the amount of decrease was less substantial than that for facial nucleus size, indicating that the reduction in the area of the facial nuclei was not due to overall shrinkage of the entire embryo after exposure to VPA. Moreover, the quantified decrease in facial nucleus area suggests an even larger percent decrease in volume: if the shape of the facial nucleus is assumed to be a sphere, then a 28.4% decrease in area equates to about a 40% decrease in volume. Thus, the total size of the facial nuclei is considerably reduced in animals exposed to VPA.

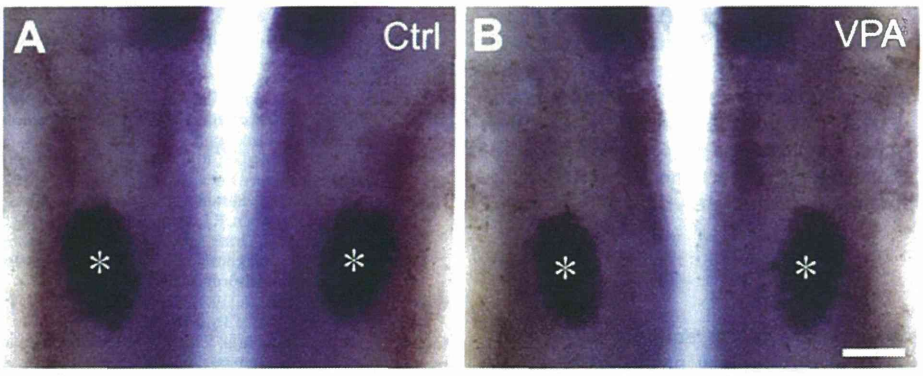

Fig. 5. *Cdh8* expression in the facial nuclei. (A and B) E15.5 preparation, viewed from the pial side, showing *cdh8*-positive facial nuclei in the control group (A) and VPA-exposed group (B). The facial nuclei are smaller in embryos exposed to VPA (B, asterisks) than in control embryos (A, asterisks). Note that *cdh8* signals were not detected in the migratory pathway (see also Fig. 3A and B, arrowheads). Rostral is up. Scale bar: 250 μm.

The reduction in facial nucleus size could be attributed to hindered cell migration, as we observed cells stacked in the migratory pathway, a common characteristic of failed cell migration, in addition to the observed inverse correlation between larger migratory pathway area and smaller facial nucleus size. Accumulating *in vivo* and *in vitro* studies have begun to elucidate the molecular mechanisms underlying the regulation of the caudal migration of neurons to facial motor nuclei in normal fishes and rodents (Bingham et al., 2002; McKay et al., 1997; Song et al., 2006; Studer et al., 1996; Wada et al., 2006). Some cell adhesion molecules, such as cadherin family members (LaMora and Voigt, 2009; Qu et al., 2010), could contribute to this migration by acting as scaffolds or facilitating the interactions between substrates. Therefore, a slight decrease in *cdh8* expression might lead to smaller facial nuclei by disrupting cellular migration. A decrease in *cdh8* expression may also explain the observed defasciculation and misrouting of peripheral facial nerves in the 2nd branchial arch (Tashiro et al., 2011), although the complimentary expression of other adhesion molecules would presumably regulate morphological development in peripheral and central facial nerve regions.

Another possible explanation for the reduction in facial nucleus size is a decreased number of cells within the nuclei given that the birth dates of most of these nuclei correspond to the stage at which VPA treatment was administered. VPA is known to affect cell division and the cell cycle by disturbing histone deacetylation (Chen et al., 2007; Phiel et al., 2001). The neurons of the facial nuclei are produced between days E12 and E14, with peak production at E13 (Altman and Bayer, 1982). In the present study, VPA exposure was performed at E9.5, and the short pharmacokinetic half-life of VPA in rodents (Nau et al., 1981) suggests that the effects of VPA would be limited to a narrow temporal window. Therefore, VPA treatment may reduce the number of early progenitor cells responsible for producing facial neurons. Further analysis of nucleogenesis is needed to clarify this possibility.

The mechanism by which VPA exposure affects the regulation of cell migration or differentiation remains unknown. It is possible that VPA exposure could have changed the identity of the rhombomeres. Various combinations of *Hox* gene expression are used to specify individual rhombomeres as well as to regulate the differentiation of cranial neurons (Erzurumlu et al., 2010; Noden, 1993; Trainor and Krumlauf, 2000; Yamamoto and Schwarting, 1991), and VPA exposure has been shown to alter the expression of *Hoxa1* (Stodgell et al., 2006). These reports support the hypothesis that VPA can change the identity of the rhombomeres. In addition, retinoic acid also contributes to the caudalization of the rhombencephalon (Altmann and Brivanlou, 2001; Glover et al., 2006; Yamada, 1994) and alters *Hox* gene expression (Conlon and Rossant, 1992; Langston and Gudas, 1992). Thus, VPA might affect retinoic acid signaling, which in turn regulates *Hox* gene expression.

In chicken embryos exposed to VPA *in ovo*, *Pax6* expression in the eye is diminished (Whitsel et al., 2002), indicating that VPA exposure can alter the expression of *Pax6*. Given that *Pax6* regulates the specification of ventral neuron subtypes in the hindbrain (Takahashi and Osumi, 2002), it is possible that VPA affects the differentiation of facial motor neurons *via Pax6* signaling. These reports indicate that VPA exposure affects the environment in which facial neurons differentiate and migrate within the hindbrain during development.

4.3. Clinical significance

In the present study, exposure of rat embryos to VPA at E9.5 affected the development of the facial nuclei in the hindbrain. In our previous study, we showed that exposure to VPA at E9.5 also affected the development of the peripheral facial nerve (Tashiro et al., 2011). Therefore, VPA exposure at E9.5 affects the development of the entire facial nerve. The embryonic stage E9.5 in rat corresponds to the 3rd week of human gestation. Pregnant women administered VPA, which is used as an anticonvulsant and mood-stabilizing drug, during this stage, sometimes give birth to children with fatal valproate syndrome or autism (Ehlers et al., 1992; Miller et al., 2005). The pharmacokinetic half-life of VPA in humans is 10-fold longer than it is in rodents (Nau et al., 1981), suggesting that the effects of VPA exposure on the development of the facial nerves that we observed in the rat would be more pronounced in humans. Our observations will contribute to the overall understanding of embryonic facial nerve development, and may be used to determine the appropriate conditions for drug administration during pregnancy.

Little is known about the capacity of abnormal morphogenesis during these early stages to cause postnatal physiological dysfunction. In autism patients, disordered caudal migration during the development of the facial nerve nuclei was shown to cause facial disease (Rodier et al., 1996). Analysis of eye-blink in a rat model of autism induced by VPA exposure might help to determine the level of function of the facial nerve. These and future findings may aid in the elucidation of the mechanisms underlying multiple inherent diseases.

Acknowledgments

We thank Thaddeus Dryja for useful comments on this manuscript. This study was supported by the Ministry of Health, Labor and Welfare of the Japanese Government and a Grand-in-Aid from the School of Medicine, Mie University.

References

Altman, J., Bayer, S.A., 1982. Development of the cranial nerve ganglia and related nuclei in the rat. Advances in Anatomy, Embryology and Cell Biology 74, 1–90.
Altmann, C.R., Brivanlou, A.H., 2001. Neural patterning in the vertebrate embryo. International Review of Cytology 203, 447–482.
Bingham, S., Higashijima, S., Okamoto, H., Chandrasekhar, A., 2002. The zebrafish trilobite gene is essential for tangential migration of branchiomotor neurons. Developmental Biology 242, 149–160.
Bloch-Gallego, E., Causeret, F., Ezan, F., Backer, S., Hidalgo-Sánchez, M., 2005. Development of precerebellar nuclei: instructive factors and intracellular mediators in neuronal migration, survival and axon pathfinding. Brain Research. Brain Research Reviews 49, 253–266.
Chandrasekhar, A., 2004. Turning heads: development of vertebrate branchiomotor neurons. Developmental Dynamics 229, 143–161.
Charman, T., Baird, G., 2002. Practitioner review: diagnosis of autism spectrum disorder in 2- and 3-year-old children. Journal of Child Psychology and Psychiatry 43, 289–305.
Chen, P.S., Wang, C.C., Bortner, C.D., Peng, G.S., Wu, X., Pang, H., Lu, R.B., Gean, P.W., Chuang, D.M., Hong, J.S., 2007. Valproic acid and other histone deacetylase inhibitors induce microglial apoptosis and attenuate lipopolysaccharide-induced dopaminergic neurotoxicity. Neuroscience 149, 203–212.
Chédotal, A., Rijli, F.M., 2009. Transcriptional regulation of tangential neuronal migration in the developing forebrain. Current Opinion in Neurobiology 19, 139–145.
Chédotal, A., 2010. Should I stay or should I go? Becoming a granule cell. Trends in Neurosciences 33, 163–172.
Conlon, R.A., Rossant, J., 1992. Exogenous retinoic acid rapidly induces anterior ectopic expression of murine *Hox-2* genes in vivo. Development 116, 357–368.
Ehlers, K., Sturje, H., Merker, H.J., Nau, H., 1992. Valproic acid-induced spina bifida: a mouse model. Teratology 45, 145–154.
Erzurumlu, R.S., Murakami, Y., Rijli, F.M., 2010. Mapping the face in the somatosensory brainstem. Nature Reviews Neuroscience 11, 252–263.
Filipek, P.A., Accardo, P.J., Baranek, G.T., Cook, E.H., Dawson, G., Gordon, B., Gravel, J.S., Johnson, C.P., Kallen, R.J., Levy, S.E., Minshew, N.J., Ozonoff, S., Prizant, B.M., Rapin, I., Rogers, S.J., Stone, W.L., Teplin, S., Tuchman, R.F., Volkmar, F.R., 1999. The screening and diagnosis of autistic spectrum disorders. Journal of Autism and Developmental Disorders 29, 439–484.
Gillberg, C., Winnergård, I., 1984. Childhood psychosis in a case of Moebius syndrome. Neuropediatrics 15, 147–149.
Glover, J.C., Renaud, J.S., Rijli, F.M., 2006. Retinoic acid and hindbrain patterning. Journal of Neurobiology 66, 705–725.
Hatten, M.E., 1999. Central nervous system neuronal migration. Annual Review of Neuroscience 22, 511–539.
Huang, Z., 2009. Molecular regulation of neuronal migration during neocortical development. Molecular and Cellular Neurosciences 42, 11–22.

Ingram, J.L., Peckham, S.M., Tisdale, B., Rodier, P.M., 2000. Prenatal exposure of rats to valproic acid reproduces the cerebellar anomalies associated with autism. Neurotoxicology and Teratology 22, 319–324.
Korematsu, K., Redies, C., 1997. Expression of *cadherin-8* mRNA in the developing mouse central nervous system. Journal of Comparative Neurology 387, 291–306.
Kraus, F., Haenig, B., Kispert, A., 2001. Cloning and expression analysis of the mouse T-box gene *Tbx20*. Mechanisms of Development 100, 87–91.
LaMora, A., Voigt, M.M., 2009. Cranial sensory ganglia neurons require intrinsic N-cadherin function for guidance of afferent fibers to their final targets. Neuroscience 159, 1175–1184.
Langston, A.W., Gudas, L.J., 1992. Identification of a retinoic acid responsive enhancer 3' of the murine homeobox gene *Hox-1.6*. Mechanisms of Development 38, 217–228.
McKay, I.J., Lewis, J., Lumsden, A., 1997. Organization and development of facial motor neurons in the Kreisler mutant mouse. European Journal of Neuroscience 9, 1499–1506.
Meins, M., Henderson, D.J., Bhattacharya, S.S., Sowden, J.C., 2000. Characterization of the human *Tbx20* gene, a new member of the T-box gene family closely related to the Drosophila H15 gene. Genomics 67, 317–332.
Miller, M.T., Strömland, K., Ventura, L., Johansson, M., Bandim, J.M., Gillberg, C., 2005. Autism associated with conditions characterized by developmental errors in early embryogenesis: a mini review. International Journal of Developmental Neuroscience 23, 201–219.
Miyazaki, K., Narita, N., Narita, M., 2005. Maternal administration of thalidomide or valproic acid causes abnormal serotonergic neurons in the offspring: implication for pathogenesis of autism. International Journal of Developmental Neuroscience 23, 287–297.
Narita, M., Oyabu, A., Imura, Y., Kamada, N., Yokoyama, T., Tano, K., Uchida, A., Narita, N., 2010. Nonexploratory movement and behavioral alterations in a thalidomide or valproic acid-induced autism model rat. Neuroscience Research 66, 2–6.
Narita, N., Kato, M., Tazoe, M., Miyazaki, K., Narita, M., Okado, N., 2002. Increased monoamine concentration in the brain and blood of fetal thalidomide- and valproic acid-exposed rat: putative animal models for autism. Pediatric Research 52, 576–579.
Nau, H., Zierer, R., Spielmann, H., Neubert, D., Gansau, C., 1981. A new model for embryotoxicity testing: teratogenicity and pharmacokinetics of valproic acid following constant-rate administration in the mouse using human therapeutic drug and metabolite concentrations. Life Sciences 29, 2803–2814.
Nieto, M.A., Patel, K., Wilkinson, D.G., 1996. In situ hybridization analysis of chick embryos in whole mount and tissue sections. Methods in Cell Biology 51, 219–235.
Noden, D.M., 1993. Spatial integration among cells forming the cranial peripheral nervous system. Journal of Neurobiology 24, 248–261.
Ornitz, E.M., Guthrie, D., Farley, A.H., 1977. The early development of autistic children. Journal of Autism and Childhood Schizophrenia 7, 207–229.
Ornoy, A., 2009. Valproic acid in pregnancy: how much are we endangering the embryo and fetus? Reproductive Toxicology 28, 1–10.
Phiel, C.J., Zhang, F., Huang, E.Y., Guenther, M.G., Lazar, M.A., Klein, P.S., 2001. Histone deacetylase is a direct target of valproic acid, a potent anticonvulsant, mood stabilizer, and teratogen. Journal of Biological Chemistry 276, 36734–36741.
Qu, Y.B., Glasco, D.M., Zhou, L.B., Sawant, A., Ravni, A., Fritzsch, B., Damrau, C., Murdoch, J.N., Evans, S., Pfaff, S.L., Formstone, C., Goffinet, A.M., Chandrasekhar, A., Tissir, F., 2010. Atypical cadherins Celsr1–3 differentially regulate migration of facial branchiomotor neurons in mice. Journal of Neuroscience 30, 9392–9401.
Rodier, P.M., Ingram, J.L., Tisdale, B., Nelson, S., Romano, J., 1996. Embryological origin for autism: developmental anomalies of the cranial nerve motor nuclei. Journal of Comparative Neurology 370, 247–261.
Rodier, P.M., Bryson, S.E., Welch, J.P., 1997. Minor malformations and physical measurements in autism: data from Nova Scotia. Teratology 55, 319–325.
Song, M.R., Shirasaki, R., Cai, C.L., Ruiz, E.C., Evans, S.M., Lee, S.K., Pfaff, S.L., 2006. T-Box transcription factor *Tbx20* regulates a genetic program for cranial motor neuron cell body migration. Development 133, 4945–4955.
Stodgell, C.J., Ingram, J.L., O'Bara, M., Tisdale, B.K., Nau, H., Rodier, P.M., 2006. Induction of the homeotic gene *Hoxa1* through valproic acid's teratogenic mechanism of action. Neurotoxicology and Teratology 28, 617–624.
Strömland, K., Nordin, V., Miller, M., Akerström, B., Gillberg, C., 1994. Autism in thalidomide embryopathy: a population study. Developmental Medicine and Child Neurology 36, 351–356.
Studer, M., Lumsden, A., Ariza-McNaughton, L., Bradley, A., Krumlauf, R., 1996. Altered segmental identity and abnormal migration of motor neurons in mice lacking *Hoxb-1*. Nature 384, 630–634.
Takahashi, M., Osumi, N., 2002. *Pax6* regulates specification of ventral neurone subtypes in the hindbrain by establishing progenitor domains. Development 129, 1327–1338.
Tashiro, Y., Endo, T., Shirasaki, R., Miyahara, M., Heizmann, C.W., Murakami, F., 2000. Afferents of cranial sensory ganglia pathfind to their target inadependent of the site of entry into the hindbrain. Journal of Comparative Neurology 417, 491–500.
Tashiro, Y., Yanagawa, Y., Obata, K., Murakami, F., 2007. Development and migration of GABAergic neurons in the mouse myelencephalon. Journal of Comparative Neurology 503, 260–269.
Tashiro, Y., Oyabu, A., Imura, Y., Uchida, A., Narita, N., Narita, M., 2011. Morphological abnormalities of embryonic cranial nerves after in utero exposure to valproic acid: implications for the pathogenesis of autism with multiple developmental anomalies. International Journal of Developmental Neuroscience 29, 359–364.
Trainor, P.A., Krumlauf, R., 2000. Patterning the cranial neural crest: hindbrain segmentation and *Hox* gene plasticity. Nature Reviews Neuroscience 1, 116–124.
Wada, H., Tanaka, H., Nakayama, S., Iwasaki, M., Okamoto, H., 2006. Frizzled3a and Celsr2 function in the neuroepithelium to regulate migration of facial motor neurons in the developing zebrafish hindbrain. Development 133, 4749–4759.
Whitsel, A.L., Johnson, C.B., Forehand, C.J., 2002. An in ovo chicken model to study the systemic and localized teratogenic effects of valproic acid. Teratology 66, 153–163.
Williams, G., King, J., Cunningham, M., Stephan, M., Kerr, B., Hersh, J.H., 2001. Fetal valproate syndrome and autism: additional evidence of an association. Developmental Medicine and Child Neurology 43, 202–206.
Yamada, T., 1994. Caudalization by the amphibian organizer: brachyury, convergent extension and retinoic acid. Development 120, 3051–3062.
Yamamoto, M., Schwarting, G., 1991. The formation of axonal pathways in developing cranial nerves. Neuroscience Research 11, 229–260.

Journal of Pediatric Neurology 10 (2012) 87–94
DOI 10.3233/JPN-2012-0541
IOS Press

Impaired prefrontal cortical response by switching stimuli in autism spectrum disorders

Naoko Narita[a,*], Akiyuki Saotome[a], Hiroki Higuchi[a], Masaaki Narita[b], Mami Tazoe[c] and Kaoru Sakatani[d]
[a]*Institute of Education, Bunkyo University, Saitama, Japan*
[b]*Developmental and Regenerative Medicine, Mie University, Mie, Japan*
[c]*Department of Clinical Psychology, Japan Lutheran College, Tokyo, Japan*
[d]*Department of Neurological Surgery, Nihon University School of Medicine, Tokyo, Japan*

Received: 2 May 2011
Revised: 21 June 2011
Accepted: 27 June 2011

Abstract. Working memory (WM) performance is considered to change according to the nature of the task by adequate and prompt activation of corresponding functional connectivity in the brain. In the present study, we examined continuous prefrontal hemodynamic changes depending on reciprocal disposition of WM and non-WM tasks using two-channel near-infrared spectroscopy. To investigate possible functional connectivity deficits in autism spectrum disorder (ASD) during these tasks, relative concentration changes in oxygenated hemoglobin (Hb), deoxygenated Hb, and total Hb were compared between high-functioning ASD subjects (n = 11) and controls (n = 22). Instant evoked cerebral blood oxygenation changes were observed in response to the task switch in controls but not in ASD subjects, although the task performance rate was almost equivalent. Delayed or altered response of functional connectivity to incoming stimuli is considered a characteristic feature of ASD.

Keywords: Autism, executive function, working memory, default mode network

1. Introduction

Autism spectrum disorder (ASD) is a set of disorders associated with intercommunication and interrelation abilities that lead to impaired cognitive and emotional development [1,2]. Furthermore, functions of higher brain networks, such as theory of mind, central coherence, and executive functions are deficient to varying extents [3]. Although numerous studies on functional neuroimaging have been conducted [4–6], clear and consistent interpretation of the defects in the prefrontal cortex (PFC) and its signal processing have not been well understood until date.

*Correspondence: Dr. Naoko Narita, Institute of Education, Bunkyo University, 3337 Minamiogishima, 343-8511, Koshigaya-City, Saitama, Japan. Tel.: +81 489 7488 11; Fax: +81 489 748 960; E-mail: nnarita@koshigaya.bunkyo.ac.jp.

Working memory (WM) is an executive function related not only to brief information retention but also to information manipulation for problem solving, planning, and language processing [7]. Advanced neuroimaging studies involving healthy individuals have shown that the dorsolateral PFC (DLPFC) and multiple other brain regions are activated during WM functioning [8–10]. On the other hand, with ASD subjects results have been inconsistent and appear to depend largely on the nature of the task and profile. Some studies have reported certain deficits of spatial WM in ASD [11–13], while others lack evidence of inferior WM performance in ASD subjects compared to that in controls [14–16]. However, studies using functional magnetic resonance imaging (fMRI) almost invariably encountered lower DLPFC activation in ASD subjects than in controls, regardless of the task

performance rate [17,18]. This behavioral-neurofunctional discrepancy may be partially explained by a functional connectivity point of view. Functional connectivity techniques help us understand how brain regions contribute to functionally connect simultaneous circuits during a task [19].

Functional connectivity is generally systematically controlled. During the resting state, a network, including the medial PFC, is activated as a default mode network (DMN). When external cognitive demanding stimuli are received the dorsal attention network, including DLPFC is activated instead of DMN being deactivated [20]. DMN deactivation was found to be disrupted in ASD, which appears to coincide with DLPFC hypoactivation when compared to the resting state on fMRI [21,22].

Recently we used near-infrared spectroscopy (NIRS) to obtain numerous noninvasive measurements of regional cerebral blood oxygenation (CBO) in vivo [23–25]. This is advantageous because the portable nature of NIRS also enables reproduction of natural experimental conditions when providing continuous and repetitive stimuli to subjects [26,27].

We hypothesized that if ASD subjects have deficiencies in functional connectivity and appropriate activation-deactivation responses to incoming variable stimuli, continuous neurophysiological monitoring would reveal a delayed and/or defective response to frequent switching of tasks of a different nature. Therefore, in this study we used NIRS measurement of CBO in PFC during switching of WM and non-WM requiring repetitive stimulation and compared relative oxygenation changes in response to stimuli switches between ASD subjects and healthy controls.

2. Materials and methods

2.1. Participants

Eleven ASD subjects intelligence quotient (IQ) > 65 according to the Wechsler intelligence scale for children-III; aged 14–46 years (mean, 29.5 years); three males and eight females; (all right-handed) and 22 healthy controls aged 19–51 years (mean, 25.2 years); six males and 16 females; (20 right-handed; two left-handed) were examined. All subjects were diagnosed (Narita Naoko and Narita Masaaki) and assessed (Tazoe Mami) by pediatric neurologists and psychologists on the basis of developmental history and current presentation according to the diagnostic and statistical manual of mental disorders IV and the Japanese version of the autism diagnostic interview-revised. The study was approved by the research and ethics committee of Bunkyo University, and written informed consent was obtained from all subjects or their legal guardians prior to the study.

2.2. Methods

The task-switching paradigm was designed using randomized geometrical figures in combinations of three shapes (circle, triangle and square) and four colors (red, yellow, blue and green). The paradigm was originally constructed using commercial presentation software (PowerPoint 2003, Microsoft, USA) and was presented to the subjects using an automated slideshow on a personal computer (Fig. 1). For the tasks that required WM (WM task), the subjects were instructed to memorize figures that appeared one by one every 3 sec on the screen (WM stimuli) and to explore and touch the figures in consecutive order as memorized within the next 15 seconds from a multiple choice panel that appeared on the screen (WM exploration). For the tasks that did not require WM (NWM task), all test figures appeared at the same time in an inset together with multiple choices on the same screen. The subjects were instructed to explore and touch the figures in the correct order as they appeared in the inset by touching the screen within 15 sec (NWM exploration). For both tasks, the number of figures presented was increased in order from one to six (described as task 1, task 2, etc.), and the tasks were programmed and performed in WM-NWM order.

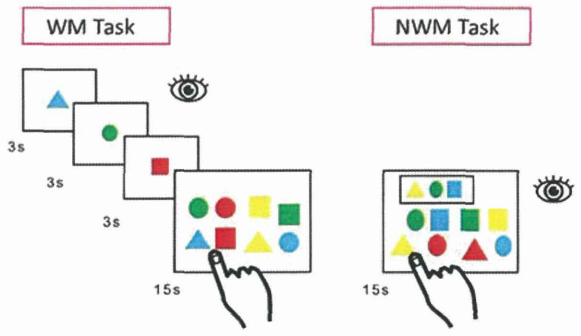

Fig. 1. An example illustration of the No. 3 task block of the experimental paradigm. After showing the subjects 3 geometrical shapes on the screen for 3 sec each (working memory [WM] stimuli), eight shapes are, shown for 15 sec and the subjects then search for and choose the shapes that they just memorized (WM exploration time). NWM exploration is, presented for 15 sec successively.

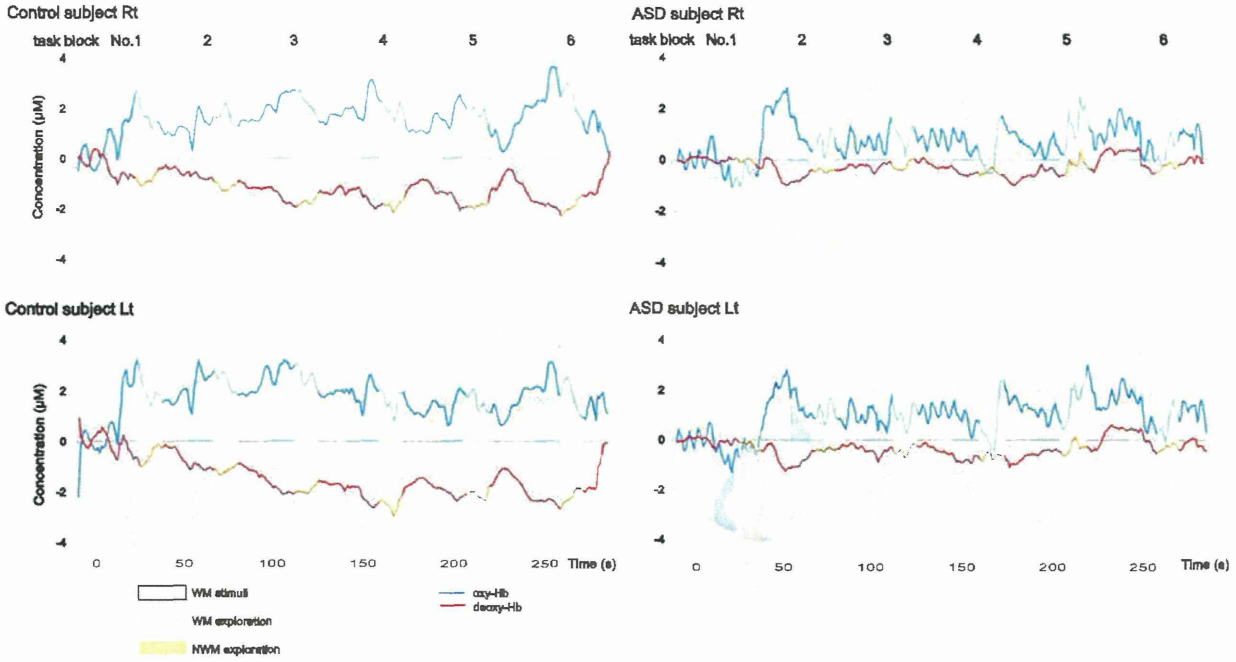

Fig. 2. Typical patterns of cerebral blood oxygenation changes measured by near-infrared spectroscopy in a control (46-year-old female subject) and an autism spectrum disorder patient (46-year-old female subject with high-functioning autistic syndrome). The right (top) and left (bottom) cerebral blood oxygenation changes in oxy-hemoglobin (blue lines) and deoxy-hemoglobin (red lines) are, indicated as relative values in units of μM. The periods of each task are color-coded. The numbers above indicate the task block number.

To facilitate calculation of task performance rate, we recorded the screen during the entire set of paradigm performances and the percentage of correct answers for each task was calculated after analyzing the tapes. The differences between WM and NWM tasks as well as between controls and ASD subjects were compared.

We measured evoked CBO changes using NIRO-200 (Hamamatsu Photonics K.K., Hamamatsu, Japan) as in our previous NIRS activation studies [27–29]. The sensors were placed symmetrically on the forehead and the midpoint between the two optodes was identical to the Fp2 position of the international electroencephalography 10/20 system [30]. Our previous MRI observations demonstrated that the emitter/detector should be placed over the frontal lobe, matching Brodmann's areas 8/9 of PFC [23], where near infrared light was and suspected to penetrate the depth of the cortical surface [31]. During performance of the switching task, concentration changes in oxygenated (oxy-) hemoglobin (Hb), deoxygenated (deoxy-) Hb, and total Hb were continuously measured with a time resolution of 1 sec.

For data analysis, baseline corrections were performed by subtracting an individual average baseline period from the value measured during each task. Then, the average Hb concentration in the 15-sec exploration periods during each task (WM and NWM) was calculated. Finally, relative value changes between corresponding WM and NWM exploration periods were evaluated by statistical analysis.

3. Results

Among the 11 ASD subjects, nine were diagnosed with Asperger syndrome and two with high-functioning autistic disorder. The mean full scale IQ was 99.4 (range 73–118), mean verbal IQ was 107.6 (89–120), and mean performance IQ was 89.5 (54–118) among ASD subjects according to Wechsler intelligence scale for children-III.

While recording NIRS data for a typical control subject, an increase in the oxy-Hb concentration was observed during the WM exploration period together with a decrease in the deoxy-Hb concentration (Fig. 2, left side panels). The oxy-Hb concentration decreased during the succeeding 15 sec of the NWM exploration period and further decreased in the subsequent WM presentation period. This tendency was most obvious

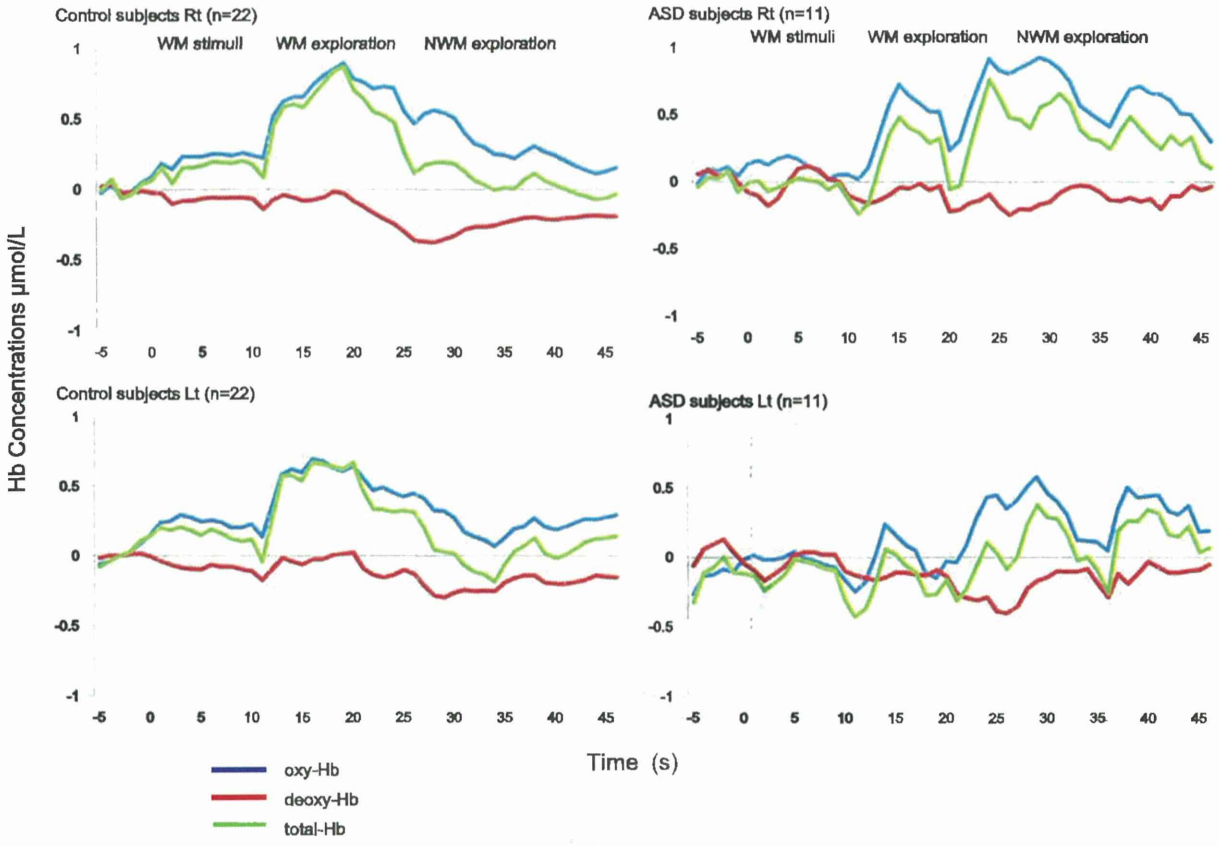

Fig. 3. The near-infrared spectroscopy data of task block No.3 was extracted and averaged for the groups. The left panels (upper panel: right prefrontal cortex, lower panel: left prefrontal cortex) represent the average oxy-hemoglobin (Hb) (blue lines), deoxy-Hb (red lines), and total Hb (green lines) concentration changes as a function of task switch in the controls. The right panels show the same results for the autism spectrum disorder subjects.

in task blocks 3, 4 and 5, and was observed in the right and left PFC. In contrast, changes in the oxy-Hb concentration according to task processing were not obvious in ASD subjects (Fig. 2, right side panels).

To further assess this difference between controls and ASD subjects, the data were reanalyzed with baseline correction by extracting only task block 3 for each subject and the average values in each group were then plotted as shown in Fig. 3. Clear discrimination of PFC activation pattern according to the task switch (i.e., WM stimuli-WM exploration-NWM exploration) observed in controls was absent in ASD subjects.

To assess the effect of task switching on hemodynamics, we calculated the mean oxy-Hb concentration of the 15-sec exploration period for each task (WM and NWM). Figure 4 shows the task wise changes in the mean oxy-Hb concentration in both the right and left sides of PFC (task blocks 1–6 of the WM-NWM task sets) of controls (Fig. 4, left side panel) and ASD subjects (Fig. 4, right side panel). In controls, the mean oxy-Hb concentration increased during WM, decreased during NWM, and gradually increased with an increase in task block number, suggesting that in the control PFC, hemodynamic activity significantly changed as memory load increased according to the task switch. In addition, right PFC laterality was, consistently observed in controls, which is predictable from the nature of the task paradigm that required spatial cognition. In contrast, ASD subjects did not show clear changes in PFC oxygenation according to the WM-NWM switch and obvious right PFC laterality was not observed.

Statistical analysis using the Mann-Whitney-Wilcoxon test was performed to compare the task-switching effect between corresponding WM-NWM task sets in the same task block. As shown, in Fig. 4, among the control subjects, the WM-NWM compar-

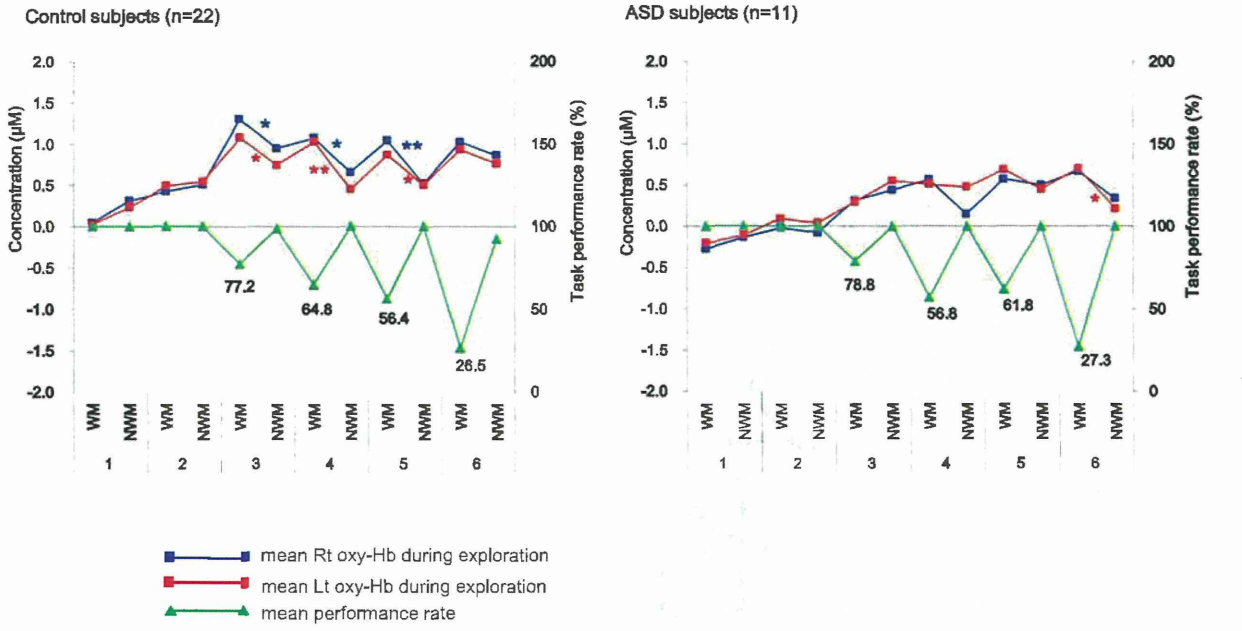

Fig. 4. The mean oxy-hemoglobin (blue lines: right prefrontal cortex, red lines: left prefrontal cortex) concentrations during the exploration period of each task and the task performance rates (green lines) are shown. Left panel: controls, Right panel: Autism spectrum disorder subjects. The left longitudinal axis indicates the relative oxy-hemoglobin concentration (μM), and the right axis indicates the task performance rate (%). The error bar indicates the standard error of the mean.

ison for task blocks 3 (Rt: $P = 0.017$, $Z = -2.386$; Lt: $P = 0.017$, $Z = -2.386$), 4 (Rt: $P = 0.014$, $Z = -2.451$; Lt: $P = 0.004$, $Z = -2.906$) and 5 (Rt: $P = 0.003$, $Z = -3.003$; Lt: $P = 0.039$, $Z = -2.062$) showed a significant difference in the oxy-Hb concentration for both the right and left PFCs. In ASD subjects, a significant difference was only detected in task block 6 for left PFC ($P = 0.021$, $Z = -2.312$).

The mean task performance rate was calculated among the groups. Both controls and ASD subjects showed a gradual decrease in the task performance rate with increasing task block number during the WM task in contrast to that during the NWM task, which was almost 100% for each task block (Fig. 4). ASD subjects showed an insignificant slightly higher mean task performance rate in task blocks 3, 5 and 6 compared to controls.

4. Discussion

In this study using NIRS, we demonstrated the tendency of an evoked CBO increase and decrease in response to task switching in the control subjects but not in ASD subjects. The switching paradigm used alternating WM and NWM tasks and the WM tasks progressively increased memory load. A significant difference in the mean oxy-Hb concentration was observed between WM and NWM exploration periods in task blocks 3, 4 and 5, which suggest that these WM tasks particularly induced a rapid regional CBO increase in the prefrontal measurement areas, which was quickly terminated with subsequent NWM task initiation.

This tendency was not obvious in ASD subjects in the early task blocks of the WM-NWM tasks. However, a weak WM task-dependent oxy-Hb increase was observed from task block 5 and above, but a statistical difference between WM and NWM tasks was found only in task block 6 for the left PFC.

Despite this obvious discrepancy in PFC hemodynamics, the mean task performance rate was similar between controls and ASD subjects. In both groups, the average correct answer rate for the WM tasks gradually decreased as memory load increased, while the NWM performance rate remained almost 100% through all tasks.

These results are consistent with those from a study conducted by Ozonoff and Strayer [15], who used geometric shapes, colored boxes, and three different

WM tasks. However, their study failed to report any significant difference in performance between the autistic, Tourette syndrome, and control groups. The nature of the tasks with colored shapes and the results that showed no significant difference between ASD subjects and controls were similar to those in our study, indicating that depending on the methodology, nature of the task, and characteristics of the participants, WM task performance itself is not always impaired in ASD patients. Nevertheless, continuous functional analysis of hemodynamics during task performance in our study showed a significant difference between controls and ASD subjects, especially in the pattern of response when the task nature changed.

One possible reason for this is ectopic activation of the brain in ASD subjects. Koshino et al. [32] suggested that autistic individuals more often tend to utilize the posterior regions of the brain to solve a WM n-back task with alphabetical letters as stimuli, i.e., they rely on lower visual signal processing rather than the left temporal region of the brain. This result suggested that spatial WM task performance in ASD subjects may be observed by ectopic neural systems or that functional connectivity differs from that activated in normal subjects.

In our present study, a significant difference between WM and NWM exploration components was observed in task blocks 3, 4 and 5 for controls, which may indicate a significant change in brain usage in response to switching of the task. In fact, this is visible in NIRS as a swift hemodynamic change when task switching occurs. Of the tasks used in this study, WM stimuli and NWM exploration components are believed to require more visual processing than the WM exploration component, which mainly requires DLPFC activation [8–10]. This explains the significant change in the PFC oxy-Hb concentration on task switching in controls. Based on the observations of previous studies and the present study, our data could be interpreted as further evidence of a difference in brain signal processing between ASD subjects and controls for tasks involving executive brain functions including spatial WM, especially when memory loads are moderate.

It is interesting that ASD subjects showed no tendency toward task-dependent changes in the PFC oxy-Hb concentration during the early task blocks, but later showed a weak switching tendency (i.e., task blocks 5 and 6; significant difference only in 6, left side). Considering that higher executive functions such as planning, flexible strategy, and organized searching would be more frequently required for later WM task blocks, the PFC oxy-Hb concentration in ASD subjects during later task blocks may indicate a shift in functional connectivity usage from the posterior domain to the prefrontal domain. This shift may be caused by an overload in lower visual processing.

Another possible explanation of the difference between controls and ASD subjects is the lack of DMN regulation in ASD subjects. Daniels et al. [33] showed functional connectivity in patients with posttraumatic stress disorder during WM processing. In their study, greater connectivity was evident between the medial PFC during the verbal WM task, where it is normally suppressed during WM processing. Inadequate DMN activation (i.e., lack of deactivation due to stimuli) in ASD subjects during cognitive tasks such as the Stroop task has also been reported by Kennedy and Courchesne [21] using functional connectivity MRI. Thus, the results observed in ASD subjects may indicate an irregular activation of default mode functional connectivity in PFC.

Combining these observations and those of previous studies, it is reasonable that neurofunctional defects in ASD subjects may not only be due to hypoactivation of task responsible brain regions but also due to a complex disorder that includes DMN defects. Considering that a certain amount of PFC activation is required in response to task switching itself [34], lack of deactivation of resting functional connectivity may lead to a delay in switching and a slow response to incoming tasks in PFC. This may activate ectopic functional connectivity that includes lower WM signal processing and posterior brain activity, although this conclusion cannot be reached definitively from our two-channel NIRS data.

When evaluating the data, it should be kept in mind that NIRS measures changes in blood oxygenation, including intracranial and extracranial tissues [35], and that the measured values indicate an average within the illuminated area. Furthermore, continuous waves of NIRS do not yield absolute values for changes in the Hb concentration without information regarding the optical path length in each subject [36]. However, the changes induced by neuronal activation are believed to indicate changes in CBO and hemodynamics within the activated cortices [23,25,31]. Moreover, the optical path length was relatively homogeneous in the forehead as compared to other re-

gions of the brain, such as the frontal-temporal junction [37]. Therefore, data analysis undertaken in the present study, which only focused on relative intra-task comparison within the continuous performance of the task-switching paradigm, is valuable.

Although the number of functional neurophysiological studies using NIRS is increasing, investigations using NIRS in ASD or other relevant neuropsychological disorders are still limited. We have found only a few studies on schizophrenia patients that describe impairment in prefrontal hemodynamics during multiple tasks including visuospatial WM [38] and the Tower of Hanoi, a classic WM task [39]. These studies suggested a difference between the affected subjects and controls. However, since neither study measured continuous hemodynamic changes during the entire task session, it is difficult to discuss the relevance of ectopic activation or DMN deactivation deficiency during the task. We previously reported continuous measurement by NIRS during two different tasks [27], which enabled us to understand that drastic changes in hemodynamics could occur depending on the nature of the task.

Since one of the characteristic clinical features of ASD is the lack of normal and natural shifts in response to external stimuli [40,41], the delayed or altered switching of functional connectivity in response to incoming stimuli observed in the present study could lead to new insights into the higher executive dysfunctions of ASD. NIRS is a convenient and non-invasive tool with fewer restrictions than fMRI; it allows subjects to perform a number of task sets continuously during measurement, and it has a wide potential application in ASD research for investigating the issues underlying PFC functional connectivity related to switching stimuli. Although the present study was conducted with a limited number of subjects, it is the first to report hemodynamic changes in ASD subjects with continuous observation of PFC during the repetition of tasks of a different nature.

Further investigations should be performed in order to elucidate functional alterations in network connectivity during WM performance in ASD subjects.

Acknowledgement

We are grateful to Dr. Masahiro Tanida for technical advice regarding the present study. This work was, supported by Grants-in-Aid for Scientific Research of the Japan Society for the Promotion of Science, the Academic Research Promotion Fund in Japan, and a research grant from the Ministry of Health, Labor, and Welfare of Japan.

References

[1] Charman T, Baird G. Practitioner review: Diagnosis of autism spectrum disorder in 2- and 3-year-old children. J Child Psychol Psychiatry 2002; 43(3): 289-305.
[2] Filipek PA, Accardo PJ, Baranek GT, Cook EH Jr, Dawson G, Gordon B, et al. The screening and diagnosis of autistic spectrum disorders. J Autism Dev Disord 1999; 29(6): 439-84. Erratum in: J Autism Dev Disord 2000; 30(1): 81.
[3] Hill EL. Executive dysfunction in autism. Trends Cogn Sci 2004; 8(1): 26-32.
[4] Castelli F, Frith C, Happé F, Frith U. Autism, Asperger syndrome and brain mechanisms for the attribution of mental states to animated shapes. Brain 2002; 125(Pt 8): 1839-49.
[5] Deuel RK. Autism: a cognitive developmental riddle. Pediatr Neurol 2002; 26(5): 349-57.
[6] Happé F, Ronald A, Plomin R. Time to give up on a single explanation for autism. Nat Neurosci 2006; 9(10): 1218-20.
[7] Baddeley AD. Working memory. Oxford: Oxford University Press; 1986.
[8] Braver TS, Cohen JD, Nystrom LE, Jonides J, Smith EE, Noll DC. A parametric study of prefrontal cortex involvement in human working memory. Neuroimage 1997; 5(1): 49-62.
[9] Cabeza R, Dolcos F, Graham R, Nyberg L. Similarities and differences in the neural correlates of episodic memory retrieval and working memory. Neuroimage 2002; 16(2): 317-30.
[10] Carlson S, Martinkauppi S, Rämä P, Salli E, Korvenoja A, Aronen HJ. Distribution of cortical activation during visuospatial n-back tasks as revealed by functional magnetic resonance imaging. Cereb Cortex 1998; 8(8): 743-52.
[11] Hughes C, Russell J, Robbins TW. Evidence for executive dysfunction in autism. Neuropsychologia 1994; 32(4): 477-92.
[12] Minshew NJ, Luna B, Sweeney JA. Oculomotor evidence for neocortical systems but not cerebellar dysfunction in autism. Neurology 1999; 52(5): 917-22.
[13] Steele SD, Minshew NJ, Luna B, Sweeney JA. Spatial working memory deficits in autism. J Autism Dev Disord 2007; 37(4): 605-12.
[14] Griffith EM, Pennington BF, Wehner EA, Rogers SJ. Executive functions in young children with autism. Child Dev 1999; 70(4): 817-32.
[15] Ozonoff S, Strayer DL. Further evidence of intact working memory in autism. J Autism Dev Disord 2001; 31(3): 257-63.
[16] Russell J, Jarrold C, Henry L. Working memory in children with autism and with moderate learning difficulties. J Child Psychol Psychiatry 1996; 37(6): 673-86.
[17] Luna B, Minshew NJ, Garver KE, Lazar NA, Thulborn KR, Eddy WF, et al. Neocortical system abnormalities in autism: an fMRI study of spatial working memory. Neurology 2002; 59(6): 834-40.
[18] Ring HA, Baron-Cohen S, Wheelwright S, Williams SC, Brammer M, Andrew C, et al. Cerebral correlates of preserved cognitive skills in autism: a functional MRI study of embedded figures task performance. Brain 1999; 122(Pt 7): 1305-15.

[19] Rogers BP, Morgan VL, Newton AT, Gore JC. Assessing functional connectivity in the human brain by fMRI. Magn Reson Imaging 2007; 25(10): 1347-57.
[20] Buckner RL, Andrews-Hanna JR, Schacter DL. The brain's default network: anatomy, function, and relevance to disease. Ann N Y Acad Sci 2008; 1124: 1-38.
[21] Kennedy DP, Redcay E, Courchesne E. Failing to deactivate: resting functional abnormalities in autism. Proc Natl Acad Sci U S A 2006; 103(21): 8275-80.
[22] Kennedy DP, Courchesne E. The intrinsic functional organization of the brain is altered in autism. Neuroimage 2008; 39(4): 1877-85.
[23] Sakatani K, Xie Y, Lichty W, Li S, Zuo H. Language-activated cerebral blood oxygenation and hemodynamic changes of the left prefrontal cortex in poststroke aphasic patients: a near-infrared spectroscopy study. Stroke 1998; 29(7): 1299-304.
[24] Sakatani K, Chen S, Lichty W, Zuo H, Wang YP. Cerebral blood oxygenation changes induced by auditory stimulation in newborn infants measured by near infrared spectroscopy. Early Hum Dev 1999; 55(3): 229-36.
[25] Sakatani K, Lichty W, Xie Y, Li S, Zuo H. Effects of aging on language-activated cerebral blood oxygenation changes of the left prefrontal cortex: Near infrared spectroscopy study. J Stroke Cerebrovasc Dis 1999; 8(6): 398-403.
[26] Sakatani K, Yamashita D, Yamanaka T, Oda M, Yamashita Y, Hoshino T, et al. Changes of cerebral blood oxygenation and optical pathlength during activation and deactivation in the prefrontal cortex measured by time-resolved near infrared spectroscopy. Life Sci 2006; 78(23): 2734-41.
[27] Murata Y, Sakatani K, Hoshino T, Fujiwara N, Kano T, Nakamura S, et al. Effects of cerebral ischemia on evoked cerebral blood oxygenation responses and BOLD contrast functional MRI in stroke patients. Stroke 2006; 37(10): 2514-20.
[28] Tanida M, Sakatani K, Takano R, Tagai K. Relation between asymmetry of prefrontal cortex activities and the autonomic nervous system during a mental arithmetic task: near infrared spectroscopy study. Neurosci Lett 2004; 369(1): 69-74.
[29] Tanida M, Katsuyama M, Sakatani K. Relation between mental stress-induced prefrontal cortex activity and skin conditions: a near-infrared spectroscopy study. Brain Res 2007; 1184: 210-6.
[30] Homan RW, Herman J, Purdy P. Cerebral location of international 10-20 system electrode placement. Electroencephalogr Clin Neurophysiol 1987; 66(4): 376-82.
[31] Hock C, Villringer K, Müller-Spahn F, Wenzel R, Heekeren H, Schuh-Hofer S, et al. Decrease in parietal cerebral hemoglobin oxygenation during performance of a verbal fluency task in patients with Alzheimer's disease monitored by means of near-infrared spectroscopy (NIRS)--correlation with simultaneous rCBF-PET measurements. Brain Res 1997; 755(2): 293-303.
[32] Koshino H, Carpenter PA, Minshew NJ, Cherkassky VL, Keller TA, Just MA. Functional connectivity in an fMRI working memory task in high-functioning autism. Neuroimage 2005; 24(3): 810-21.
[33] Daniels JK, McFarlane AC, Bluhm RL, Moores KA, Clark CR, Shaw ME, et al. Switching between executive and default mode networks in posttraumatic stress disorder: alterations in functional connectivity. J Psychiatry Neurosci 2010; 35(4): 258-66.
[34] Dove A, Pollmann S, Schubert T, Wiggins CJ, von Cramon DY. Prefrontal cortex activation in task switching: an event-related fMRI study. Brain Res Cogn Brain Res 2000; 9(1): 103-9.
[35] van der Zee P, Cope M, Arridge SR, Essenpreis M, Potter LA, Edwards AD, et al. Experimentally measured optical pathlengths for the adult head, calf and forearm and the head of the newborn infant as a function of inter optode spacing. Adv Exp Med Biol 1992; 316: 143-53.
[36] Delpy DT, Cope M, van der Zee P, Arridge S, Wray S, Wyatt J. Estimation of optical pathlength through tissue from direct time of flight measurement. Phys Med Biol 1988; 33(12): 1433-42.
[37] Zhao H, Tanikawa Y, Gao F, Onodera Y, Sassaroli A, Tanaka K, et al. Maps of optical differential pathlength factor of human adult forehead, somatosensory motor and occipital regions at multi-wavelengths in NIR. Phys Med Biol 2002; 47(12): 2075-93.
[38] Quaresima V, Giosuè P, Roncone R, Casacchia M, Ferrari M. Prefrontal cortex dysfunction during cognitive tests evidenced by functional near-infrared spectroscopy. Psychiatry Res 2009; 171(3): 252-7.
[39] Ikezawa K, Iwase M, Ishii R, Azechi M, Canuet L, Ohi K, et al. Impaired regional hemodynamic response in schizophrenia during multiple prefrontal activation tasks: a two-channel near-infrared spectroscopy study. Schizophr Res 2009; 108(1-3): 93-103.
[40] Courchesne E, Townsend J, Akshoomoff NA, Saitoh O, Yeung-Courchesne R, Lincoln AJ, et al. Impairment in shifting attention in autistic and cerebellar patients. Behav Neurosci 1994; 108(5): 848-65.
[41] Robinson S, Goddard L, Dritschel B, Wisley M, Howlin P. Executive functions in children with autism spectrum disorders. Brain Cogn 2009; 71(3): 362-8.

Int. J. Devl Neuroscience 31 (2013) 751–761

Contents lists available at ScienceDirect

International Journal of Developmental Neuroscience

journal homepage: www.elsevier.com/locate/ijdevneu

Thyroid hormone-dependent development of the GABAergic pre- and post-synaptic components in the rat hippocampus

Erika Sawano[a], Masaki Takahashi[a,b], Takayuki Negishi[a,c], Tomoko Tashiro[a,*]

[a] Department of Chemistry and Biological Science, School of Science and Engineering, Aoyama Gakuin University, 5-10-1 Fuchinobe, Chou-ku, Sagamihara, Kanagawa 252-5258, Japan
[b] National Institute of Neuroscience, National Center of Neurology and Psychiatry (NCNP), 4-1-1 Ogawa-higashi, Kodaira, Tokyo 187-8502, Japan
[c] Department of Physiology, Faculty of Pharmacy, Meijo University, 150 Yagotoyama, Tempaku-ku, Nagoya, Aichi 468-8503, Japan

ARTICLE INFO

Article history:
Received 18 March 2013
Received in revised form 30 August 2013
Accepted 17 September 2013

Keywords:
Thyroid hormone
Brain development
Hippocampus
GABAergic system
GAD65
GAD67
KCC2

ABSTRACT

Thyroid hormone (TH) plays essential roles in normal brain development mainly by regulating gene expression through binding to specific nuclear receptors which serve as transcription factors. Previous studies showed that perinatal deficiency of TH or impairment of its signaling severely affect brain development, especially the development of the γ-aminobutyric acid (GABA) system, but cellular and molecular targets of the hormone are only partly uncovered. In the present study, we focused on the developing rat hippocampus which was confirmed to be one of the regions highly sensitive to TH status, and found two new targets of the hormone among the pre- and post-synaptic components of the GABAergic system. One was glutamic acid decarboxylase 65 (GAD65), the protein level of which was reduced to less than 50% of control in the hippocampus of hypothyroid rats (obtained by administering 0.025% methimazole in drinking water to pregnant dams from gestational day 15 until 4 weeks postpartum) and recovered to control levels by daily thyroxine-replacement after birth. Reduction in GAD65 protein was correlated immunohistochemically with a 37% reduction in the number of GAD65-positive cells as well as a reduction in GAD65-positive processes. In contrast, the other GAD isotype, GAD67, was not affected by TH status. A subpopulation of GABAergic neurons containing parvalbumin was also confirmed to be highly dependent on TH status. The second target of thyroid hormone was neuron-specific K^+/Cl^- co-transporter, KCC2, which is responsible for switching of GABA action from excitatory to inhibitory. In the euthyroid hippocampus, a sharp rise of *kcc2* expression was observed at postnatal day (PND)10 which was followed by a large increase in KCC2 protein at PND15. This transient rise in *kcc2* expression was completely suppressed by hypothyroidism, resulting in nearly 80% reduction in KCC2 protein at PND15. These results indicate that the development of GABAergic terminals and the excitatory to inhibitory maturation of GABA signaling are strongly dependent on TH.

1. Introduction

Thyroid hormone (TH) is essential for proper brain development. Its insufficiency during the perinatal period results in a syndrome known as cretinisim in humans which consists of mental retardation, ataxia, and deafness together with impairment of body growth. At the cellular level, relatively later processes of central nervous system (CNS) development such as neurogenesis, cell migration, axonal and dendritic proliferation, synaptogenesis, and myelination are affected by hypothyroidism (Bernal and Nunez, 1995; Oppenheimer and Schwartz, 1997; Koibuchi and Chin, 2000; Thompson and Potter, 2000; Williams, 2008).

As TH exerts its effects mainly through binding to the specific nuclear receptors of the steroid-retinoic acid-TH receptor superfamily which function as ligand-regulated transcription factors, one of the essential steps in understanding its mechanism of action is to identify genes regulated by TH. Many previous studies have focused on the rodent cerebellum as a model system since it develops postnatally during the critical time window of TH action and is severely affected by hypothyroidism. Microarray-based global gene expression analyses of the developing cerebellum from animals with altered TH status (Quignodon et al., 2007; Takahashi et al., 2008) or of cultured cerebellar neurons after addition of the transcriptionally active TH, 3,5,5′-triiodothyronine (T3) (Quignodon et al., 2007; Chatonnet et al., 2012) resulted in the identification of several new candidate genes, and chromatin immunoprecipitation assays have been carried out to directly identify TH target genes

* Corresponding author. Tel.: +81 42 759 6235; fax: +81 42 759 6235.
E-mail addresses: eri_1018_eri@hotmail.co.jp (E. Sawano), masaki_810@hotmail.com (M. Takahashi), taka-u@yayoi.club.ne.jp (T. Negishi), ttashiro@aoyamagakuin.jp (T. Tashiro).

0736-5748/$36.00 © 2013 ISDN. Published by Elsevier Ltd. All rights reserved.
http://dx.doi.org/10.1016/j.ijdevneu.2013.09.007

(Quignodon et al., 2007; Dong et al., 2009), but the total number of genes confirmed to be directly regulated by TH is still limited.

Hypothyroidism has a strong negative effect on the development of the γ-aminobutyric acid (GABA) system *in vivo* and *in vitro* (reviewed in Wiens and Trudeau, 2006), leading to impairments in GABAergic circuit formation and inhibitory neurotransmission in the cerebral cortex and the hippocampus (Gilbert et al., 2007; Friauf et al., 2008a) as well as the differentiation and development of GABAergic neurons (Manzano et al., 2007; Westerholz et al., 2010). Reduced TH signaling in TH receptor α1 (TRα1) knockout mice (Guadaño-Ferraz et al., 2003) or mice expressing mutant TRα1 with 10-fold lower affinity for TH (Venero et al., 2005; Wallis et al., 2008) results in significant reductions in GABAergic terminals in the hippocampus correlated with behavioral abnormalities. However, molecular targets of the hormone in the GABAergic system are only partly uncovered.

Since previous studies have been carried out under different experimental conditions and have focused on different regions of the brain, we first examined the differential sensitivity of the developing rat brain regions (cerebral cortex, hippocampus, striatum, midbrain, and cerebellum) toward TH status in the present study by measuring the mRNA expressions of the known TH-dependent genes. For this purpose, three genes were selected (neurogranin, hairless, myelin basic protein) which are widely expressed in the brain and well established as direct targets of T3 *in vivo*. In the hippocampus which was confirmed to be one of the highly sensitive regions to TH under the present experimental protocol, TH-dependent alterations in the amount of both pre- and post-synaptic components of the GABAergic system were further investigated.

GABA is the main inhibitory neurotransmitter in the mature CNS, but it mainly acts as an excitatory neurotransmitter during early stages of development (Ben-Ari, 2002; Payne et al., 2003; Ben-Ari et al., 2007; Farrant and Kaila, 2007). In addition to the differentiation of GABAergic neurons and establishment of the GABAergic synapses, this switching in the action of GABA is another key event in the development of the GABAergic system. It takes place around the 2nd postnatal week in rats through reduction of intracellular Cl^- concentration (Rivera et al., 1999). Since this period overlaps with the critical time window of TH-dependent growth in the CNS (Oppenheimer and Schwartz, 1997; Thompson and Potter, 2000), we further examined the TH-dependence of the expression of the neuron-specific K^+/Cl^- co-transporter (KCC2) which is responsible for excluding intracellular Cl^- and establishing low intracellular Cl^- concentration (Rivera et al., 1999; Payne et al., 2003; Fiumelli and Woodin, 2007). The results indicate that TH is essential both for the differentiation of the presynaptic GABAergic neurons and the maturation of the postsynaptic components of the GABAergic system in the developing hippocampus.

2. Materials and methods

2.1. Animal treatment

Pregnant Wistar/ST rats were purchased from SLC (Shizuoka, Japan). They were housed individually under controlled temperature (24 ± 1 °C) on a 12-h-light (06:00–18:00 h): 12-h-dark (18:00–06:00 h) cycle. Food and water were available *ad libitum*. Three pregnant dams were used to obtain pups in each of the following three treatment groups; control, hypothyroid, hypothyroid with thyroxine (T4) replacement. Hypothyroid and T4-replacement groups were rendered hypothyroid by administering 0.025% (w/v) 2-mercapto-1-methylimidazole (MMI) in drinking water to their mothers from the 15th day of conception. From the day of birth, pups from the T4-replacement group received daily subcutaneous injection of T4 (20 ng/g body weight/day) dissolved in saline while control and hypothyroid pups received saline until sacrifice 6 h after the last injection. For one series of experiments, five pups each of control, hypothyroid and T4-replacement groups were used at postnatal day (PND) 4, 10, 15 and 28. They were sacrificed under deep ether anesthesia and blood samples were drawn from the heart and collected with 5 mM EDTA as anticoagulant. After perfusion with phosphate-buffered saline (PBS), the brains were removed and separated sagitally into halves. In total, four series of animals were used to obtain tissue samples for mRNA and protein extractions and immunohistochemical observation. Five brain regions (cerebral cortex, hippocampus, striatum, midbrain and cerebellum) were excised for mRNA extractions and hippocampi were excised for protein extractions, immediately frozen in liquid N_2, and kept at −80 °C until use. For immunohistochemistry, brain halves were immediately fixed in 4% paraformaldehyde (PFA).

All animal treatments have been approved by the Animal Experimentation Committee of Aoyama-Gakuin University and were carried out under veterinary supervision and in accordance with the 'Guidelines for the Use of Animals in Neuroscience Research'.

2.2. Measurement of plasma T4 levels

Blood samples were centrifuged at 1500 × *g* for 20 min at room temperature to obtain the plasma as the supernatant. T4 in the plasma from control (n = 5–12), hypothyroid (n = 5–12) and T4-replacement groups (n = 5–11) were measured by competitive enzyme- linked immunosorbent assay (ELISA) kit (Diagnostic Automation Inc.) according to the protocols recommended by the manufacturer.

2.3. Real-time quantitative fluorescence-based PCR

Total RNA was prepared individually from five brain regions obtained from five pups of each treatment group at PND4, 10, 15 and 28, using Trizol reagent (Invitrogen Life Technologies, Carlsbad, CA). First-strand cDNA was synthesized from 2 μg total RNA from one animal using SuperScript II reverse transcription kit (Invitrogen Life Technologies). Expression levels of the following 12 genes in cDNA samples were quantified by fluorescence-based real-time PCR using Smart Cycler System (Cepheid, Sunnyvale, CA, USA) with SYBR Premix ExTaq (Takara, Shiga, Japan): cyclophilin-A (*ppia*), neurogranin (*rc3*), hairless (*hr*), reelin (*reln*), myelin basic protein (*mbp*), glutamic acid decarboxylase 65 (*gad65*), GABA(A) receptor subunit α1 (*gabra1*), GABA(A) receptor subunit β2 (*gabrb2*), GABA(A) receptor subunit γ2 (*gabrg2*), gephyrin (*gphn*), collybistin (*arhgef9*), K^+/Cl^- cotransporter (*kcc2*). Data were analyzed by $2^{-\Delta\Delta Ct}$ method using cyclophilin-A (*ppia*) as an internal standard gene, as its expression level was not affected by thyroid status (Muñoz et al., 1991) or during postnatal development (Takahashi et al., 2005). PCR primers were designed in Oligo 6.0 primer analysis software (Molecular BiologyInsights). Sequences of the PCR primers are listed in Table 1.

2.4. Western blotting

Each hippocampal sample obtained from each group at PND4, 10, 15 and 28 (n = 5 for either group at each time point) was homogenized in 10 volumes of Cel-Lytic MT (Sigma, St. Louis, MO, USA) containing protease inhibitor cocktail (Sigma), centrifuged at 12,000 × *g* for 11 min at 4 °C and supernatant was collected. Concentrations of extracted proteins in the supernatant were determined by Protein Quantification Kit – Wide Range (Dojindo Molecular Technologies, Kumamoto, Japan) before proceeding with Western blotting. Each protein extract was combined with 4× sample buffer (0.25 M Tris–HCl, 40% glycerol, 8% SDS, 0.04% bromophenol blue, 8% β-mercaptoethanol) and boiled for 5 min. Samples were separated by SDS-PAGE on Tris–HCl gels followed by electrophoretic transfer onto polyvinyl difluoride (PVDF) membranes (Millipore, Bedford, MA). The blots were blocked for 1 h at RT with 2% BSA or 2.5% skimmed milk in PBS containing 0.1% Tween 20 (PBS-T) and 0.02% sodium azide, and incubated overnight at 4 °C with one of the following primary antibodies in 2% BSA and 0.02% sodium azide-containing PBS; monoclonal anti-glutamic acid decarboxylase 65 (GAD65; 1:500; Santa Cruz Biotechnology, Santa Cruz, CA), monoclonal anti-GAD67 (1:10,000; Abcam, Cambridge, United Kingdom), rabbit polyclonal anti-K^+/Cl^- cotransporter (KCC2; 1:5000; Millipore) and monoclonal anti-β-actin (1:10,000; Sigma, St. Louis, MO). After being rinsed in PBS-T, the blots were incubated for 1 h at RT with either of the following horseradish peroxidase (HRP)-conjugated secondary antibodies in 2% BSA with 0.02% sodium azide; anti-rabbit IgG (1:5000) and anti-mouse IgG (1:10,000) (both from Jackson Immunoresearch, West Grove, PA). The blots were rinsed several times in PBS-T and visualized by exposure to Hyperfilm ECL (GE Healthcare, Buckinghamshire, United Kingdom) using an Immobilon Western Chemiluminescent HRP Substrate (Millipore). For quantification, the films were scanned, and the density of each band was measured in Image J (National Institutes of Health), and the results normalized using β-actin as standard.

2.5. Immunohistochemistry

For immunohistochemical analysis, brain samples were fixed in 4% PFA for 48 h at 4 °C, dehydrated, embedded in paraffin, and cut into 8-μm-thick coronal sections. Three consecutive sections per animal taken from identical locations in the frontal part of lateral hippocampus were used for immunohistochemical staining with three different antibodies; the first section with anti-GAD65 antibody, the second section with anti-GAD67 antibody, and the third section with anti-parvalbumin (PV) antibody. After deparaffinization and rehydration, the sections were incubated in 0.5% hydrogen peroxide (H_2O_2) for 20 min at RT to quench endogenous peroxidase activity, and boiled with 0.01 M citrate buffer for 20 min or incubated in 0.3% Triton

Table 1
Primers for real-time quantitative PCR.

	Forward	Reverse
ppia	GCAAGACCAGCAAGAAGATCACC	CTTCAGTGAGAGCAGAGATTACAG
rc3	GACTTCCCTACTGTGTTTGTGAG	CTACGCCACGACGAAGCCAGC
hr	GCTGACCCCTCCCCTCATGG	GCAGTTGAGATACACAGAGGAAG
mbp	GGCACAGAGACACGGGCATCC	GCGACTTCTGGGGCAGGGAGC
gabra1	GGGTAAGGTGAGGCTGTCATTGT	TCTGTGTTAGGCTGGCTCATCTC
gabrb2	CGATGACCACAATCAATACCCATCT	GCCATAAAGACAAAGACAAAGCACC
gabrg2	GAGTGTTTGGATGGCAAGGACTG	AAGCAGAAGGCGGTAGGGAAGAA
gphn	TGGAACTTCACAAAGGCGAG	AAAACTAGCTGTGCCGTTGC
arhgef9	GAAGGACAGCCGCTATCAAC	ATCACTGTGGTCTTGGGCAG
kcc2	CCATCCAGGTGACTTTACTCTGA	CCTCTCCTATTTACAAGGGTTTTG

X-100 for 15 min at RT to retrieve the antigen. They were rinsed in PBS and incubated in 4% BSA for 30 min at RT to block nonspecific binding sites. Rabbit polyclonal anti-GAD65 antibody (1:500; Sigma), monoclonal anti-GAD67 antibody (1:2000; Abcam) or monoclonal anti-PV antibody (1:4000; Sigma) was then applied to each section, and the sections were incubated overnight at 4 °C. They were further rinsed in PBS and incubated for 1 h at RT with either of the following biotinylated secondary antibodies in BSA/PBS; anti-mouse IgG (1:1000) and anti-rabbit IgG (1:1000) (both from Chemicon/Millipore). The sections were incubated in biotin-conjugated horseradish peroxidase with streptavidin (ABC Elite Kit; Vector, Burlingame, CA) at a dilution of 1:1000 for 30 min at RT and then visualized with nickel-intensified diaminobenzidine. The sections were dehydrated and mounted in Entellan New (Merck, Darmstadt, Germany), and observed with a microscope (Axioplan 2; Carl Zeiss, Oberkochen, Germany). The images were recorded with a color CCD camera (ProgRes; Genoptik, Jena, Germany).

2.6. Statistical analysis

All numerical data were expressed as mean ± SEM and analyzed by one-way analysis of variance (ANOVA). When ANOVA revealed significant differences, it was followed by two-tailed Student's *t*-test. Level of significance was set at $p < 0.05$.

3. Results

3.1. Confirmation of the effect of maternal MMI-treatment and postnatal T4-replacement on the plasma thyroxine level of neonatal rats

Among the three experimental groups of control, hypothyroid (MMI-treated), and hypothyroid with T4-replacement, there was no significant difference in dam's body weights, litter size, sex ratio of the offspring or survival of pups to weaning. Hypothyroid pups had body weights comparable to control pups at postnatal day 4 (PND4), but started to show reductions in body weight gain around PND7 (Fig. 1A). They also showed retardations in development such as a delay in eye opening and hair growth. Pups in the T4-replacement group showed a significant recovery of the growth curve compared with the hypothyroid group.

To confirm the hypothyroid state of the MMI-treated group and its rescue by T4-replacement, plasma T4 level was determined in animals from the three groups at PND 4, 10, 15 and 28. As shown in Fig. 1B, plasma T4 level of control pups showed a 2.7-fold increase between PND4 and 10, was maintained at this high level until PND15, and started to decline at PND28. Hypothyroid pups had a severe reduction in plasma T4 level at all time points whereas the pups in T4-replacement group had normal or higher plasma level of T4 measured 6 h after T4 injection. In particular, T4-replacement resulted in the plasma T4 level significantly higher than that of the control at PND4 when normal T4 level was still low.

3.2. Differences in sensitivities toward TH status among the developing brain regions

Since previous studies have been carried under different experimental conditions to induce hypothyroidism (such as timing

A

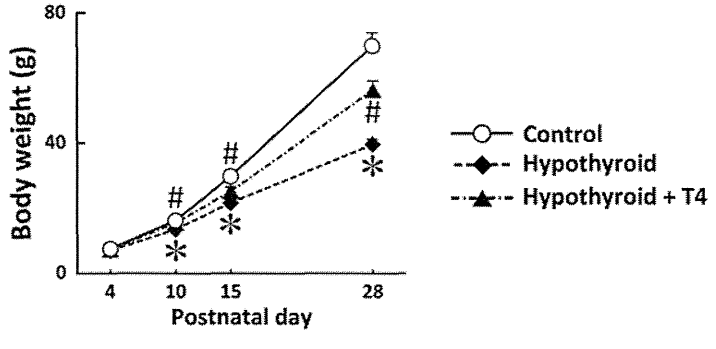

B

	Plasma levels of thyroxine (ng/ml)			
	PND4	PND10	PND15	PND28
Control	45.1 ± 1.7	121.2 ± 7.0	127.2 ± 10.2	95.6 ± 9.7
Hypothyroid	29.0 ± 2.3 *	14.8 ± 2.3 *	12.7 ± 1.0 *	21.9 ± 3.5 *
Hypothyroid + T4	79.9 ± 2.5 #	131.8 ± 9.7 #	100.2 ± 10.5 #	117.2 ± 4.1 #

Fig. 1. Body weights and plasma thyroxine (T4) levels of pups during development. (A) Body weights of control (open circles), hypothyroid (solid squares) and T4-replacement groups (solid triangles) of pups at PND4, 10, 15 and 28. Results are expressed as means + SEM. $n = 5–25$ (control group), $n = 6–30$ (hypothyroid group), $n = 10–31$ (T4-replacement group). (B) Plasma levels of T4 in the three experimental groups at PND4, 10, 15 and 28. Results are expressed as means ± SEM. $n = 5–12$ (control group, hypothyroid group, T4-replacement group). $^{*}P < 0.05$ between control and hypothyroid groups. $^{\#}P < 0.05$ between hypothyroid and T4-replacement groups.

of anti-thyroid drug treatment) and focused on different brain regions, we attempted to evaluate the differences in sensitivities toward TH status among the developing rat brain regions under the present experimental protocol by examining mRNA expression of the three known TH-responsive genes, neurogranin (*rc3*), myelin basic protein (*mbp*), and hairless (*hr*) by real-time PCR in five brain regions (cerebral cortex, hippocampus, striatum, midbrain and cerebellum) in the three groups of animals (Fig. 2). We chose these genes because they are widely expressed in the brain and their gene structures have been well characterized and shown to possess TH-responsive elements (TREs) which are functional *in vivo* (Farsetti et al., 1991; Martínez de Arrieta et al., 1999; Thompson and Bottcher, 1997).

Expression of each gene in different regions at different time points was compared pairwise between hypothyroid and control groups as well as between hypothyroid and T4-replacement groups. When the expression of a gene was significantly down-regulated in the hypothyroid group compared with the control

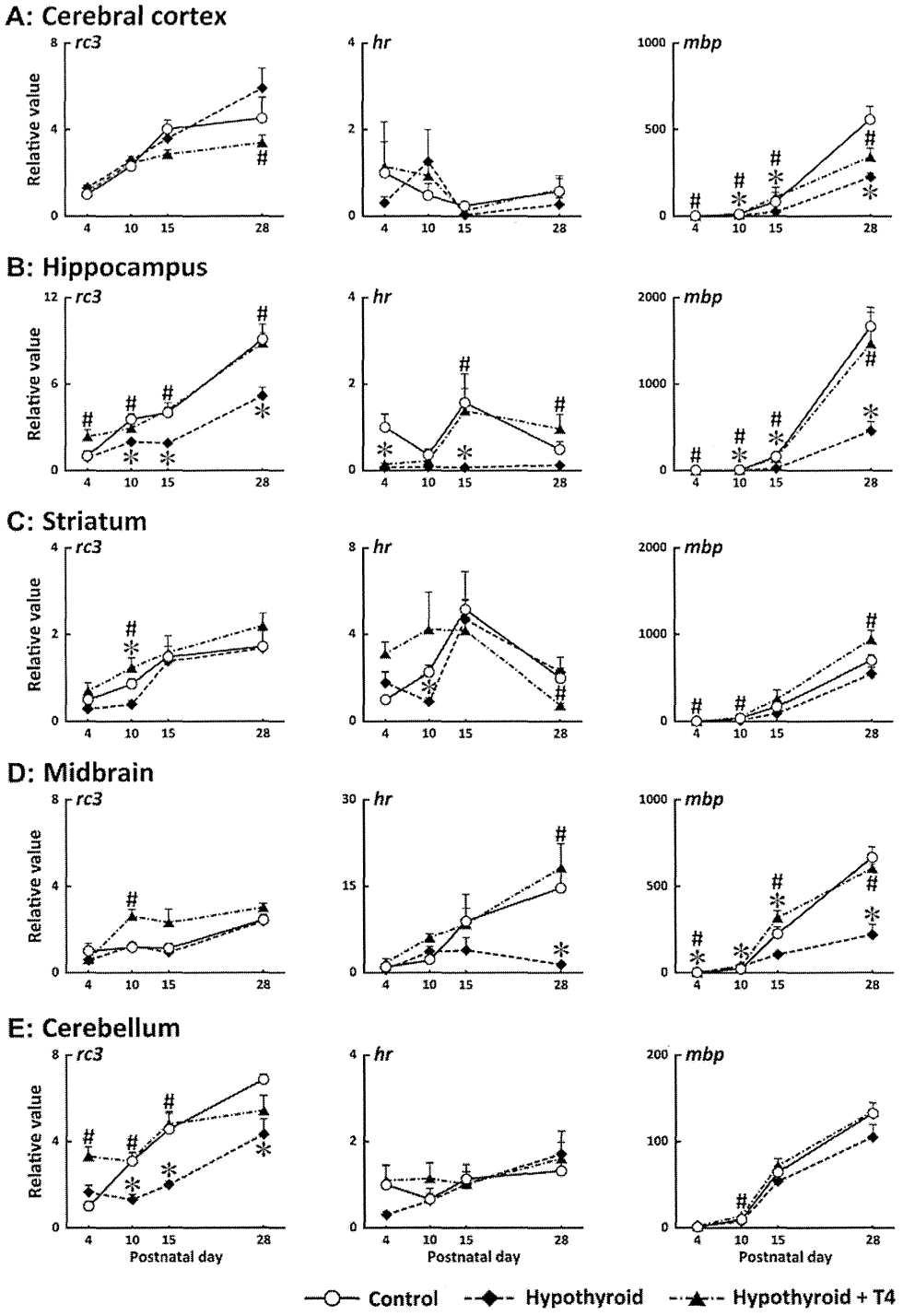

Fig. 2. Comparison of expression profiles of TH-responsive genes in the five brain regions of control, hypothyroid and T4-replacement groups during development. The mRNA expression of rc3, hr and mbp in the five brain regions (A: cerebral cortex, B: hippocampus, C: striatum, D: midbrain, E: cerebellum) of pups in the control (open circles), hypothyroid (solid squares) and T4-replacement groups (solid triangles) was quantified by real-time PCR at PND4, 10, 15 and 28 using ppia as internal standard. Each mRNA level is expressed relative to that of the control group at PND4 (means + SEM of 5 rats/group/age). $^{*}P < 0.05$ between control and hypothyroid groups. $^{\#}P < 0.05$ between hypothyroid and T4-replacement groups.

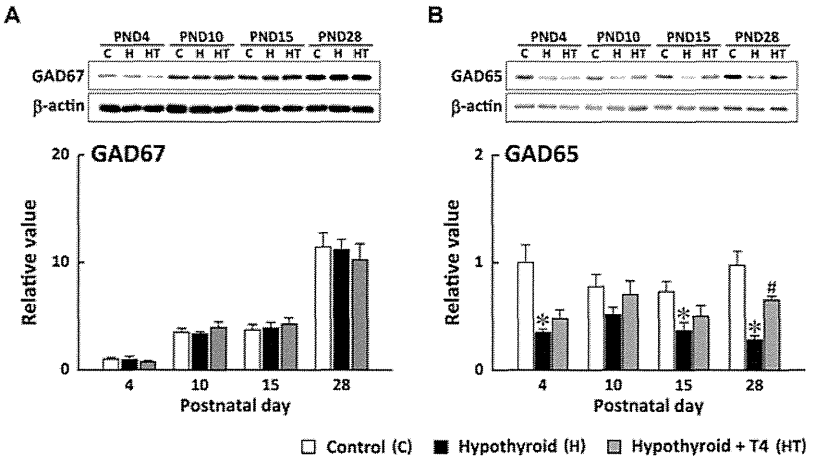

Fig. 3. GAD67 and GAD65 protein levels in the hippocampus of control, hypothyroid and T4-replacement groups during development. GAD67 (A) and GAD65 (B) protein levels were quantified by Western blotting with anti-GAD67 and anti-GAD65 antibodies, respectively. Immunoreactive bands of GAD67 and GAD65 (examples shown in upper panels) in the hippocampus of control (open bars), hypothyroid (solid bars) and T4-replacement groups (shaded bars) at different ages were quantified using β-actin as standard and expressed relative to that of the control group at PND4 (means + SEM of 5 rats/group/age). $^{*}P < 0.05$ between control and hypothyroid groups. $^{\#}P < 0.05$ between hypothyroid and T4-replacement groups.

(marked with asterisks in Fig. 2) and significantly up-regulated in the T4-replacement group compared with the hypothyroid group (marked with # in Fig. 2) at the same time, it was judged as TH-responsive expression. In the cerebral cortex (Fig. 2A), only *mbp* at PND10, 15, and 28 showed TH-responsive expression. In contrast, TH-responsive expression was observed with *rc3* and *mbp* at three time points as well as *hr* at PND15 in the hippocampus (Fig. 2B). In the striatum (Fig. 2C) and the cerebellum (Fig. 2E), only *rc3* at one (PND10) or two (PND10, 15) time points was TH-responsive, while *hr* at PND28 and *mbp* at three time points were responsive in the midbrain (Fig. 2D). The results thus showed that the hippocampus had TH-sensitivity comparable to or higher than that of the well-studied TH-sensitive regions such as the cerebellum under our experimental protocol.

3.3. Effect of TH status on the development of GABAergic neurons in the hippocampus

To examine the role of TH in the development and maturation of the GABAergic system in the hippocampus, protein expressions of the GABA-synthesizing enzymes, GAD67 and GAD65, were first compared in the three experimental groups.

The two GAD isotypes showed sharp differences in protein expression both developmentally and in response to altered TH status (Fig. 3). In the control hippocampus, the amount of GAD67 increased more than 10-fold in a biphasic manner between PND4 and 28 (Fig. 3A) whereas that of GAD65 did not change significantly during the same time (Fig. 3B). On the other hand, the amount of GAD65 responded to TH status with significant reductions in the hypothyroid compared with the control at PND4, 15, and 28. At PND28, GAD65 protein in hypothyroid pups was decreased to 29% of that in control pups, which was recovered significantly by continuous T4-replacement (Fig. 3B). In contrast, differences in the amount of GAD67 were not observed among the three experimental groups between PND4 and 28 (Fig. 3A).

To determine whether the decrease of GAD65 protein in the hypothyroid hippocampus was caused by a decrease in the number of GABAergic neurons or not, GAD67- and GAD65-positive cells in matching sections from 6 animals per experimental group were numerically evaluated by immunohistochemistry at PND28 (Figs. 4 and 5). In the control hippocampus, GAD67- or GAD65-positive cells were distributed throughout the hippocampus proper and the dentate gyrus (DG), both in the principal cell layer and other layers. The number of positive cells was largest in the CA1 subregion, followed by comparable numbers in CA3 and DG subregions. There were consistently more somata positive for GAD67 than for GAD65 as described previously (Fukuda et al., 1997). In addition to staining of GABAergic cell bodies, perisomatic staining of pyramidal cells was observed with both GAD antibodies in CA1–CA3. Staining of dendritic layers (stratum radiatum and stratum oriens) was stronger with GAD65 antibody compared with GAD67, confirming the preferential synaptic localization of GAD65 (Esclapez et al., 1994; Fukuda et al., 1998). Strong staining only with GAD67-antibody was observed along mossy fiber pathways (stratum lucidum of CA3 and hilus of the DG) as described previously (Sloviter et al., 1996; Fukuda et al., 1997; Gutiérrez et al., 2003).

There were no significant differences in the GAD67 staining or in the number of GAD67-positive cells among the three experimental groups (Fig. 4). In contrast, there was a 37% reduction in the number of GAD65-positive cells in the hypothyroid hippocampus compared to the control, which was completely recovered by T4-replacement (Fig. 5B). At the same time, GAD65 immunostaining in the principal cell layer was also reduced by hypothyroidism and recovered by T4-replacement (Fig. 5B).

A subpopulation of GABAergic neurons containing parvalbumin (PV) was also affected by perinatal hypothyroidism (Fig. 6), as previously shown in the neocortex and the hippocampus (Gilbert et al., 2007). PV-positive cells were located mainly in the pyramidal cell layer of CA1-3 and the hilar edge of the granule cell layer in DG. Their number was significantly decreased in all four subregions of the hippocampus in the hypothyroid group, resulting in a 33% reduction in total compared with the control (Fig. 6B). The number of PV-positive cells was completely recovered by T4-replacement. In addition to staining of the GABAergic cell bodies, prominent perisomatic staining of principal cells as well as clear staining of processes both in the principal cell layer and extending in the dendritic layers (stratum radiatum and stratum oriens) were observed with PV-antibody (Fig. 6A). Such non-somatic staining was also reduced by hypothyroidism and recovered by T4-replacement.

3.4. Effect of the TH status on the postsynaptic components of the GABAergic system

Paralleling the decrease in the number of pre-synaptic GABAergic neurons and their processes due to hypothyroidism, alterations

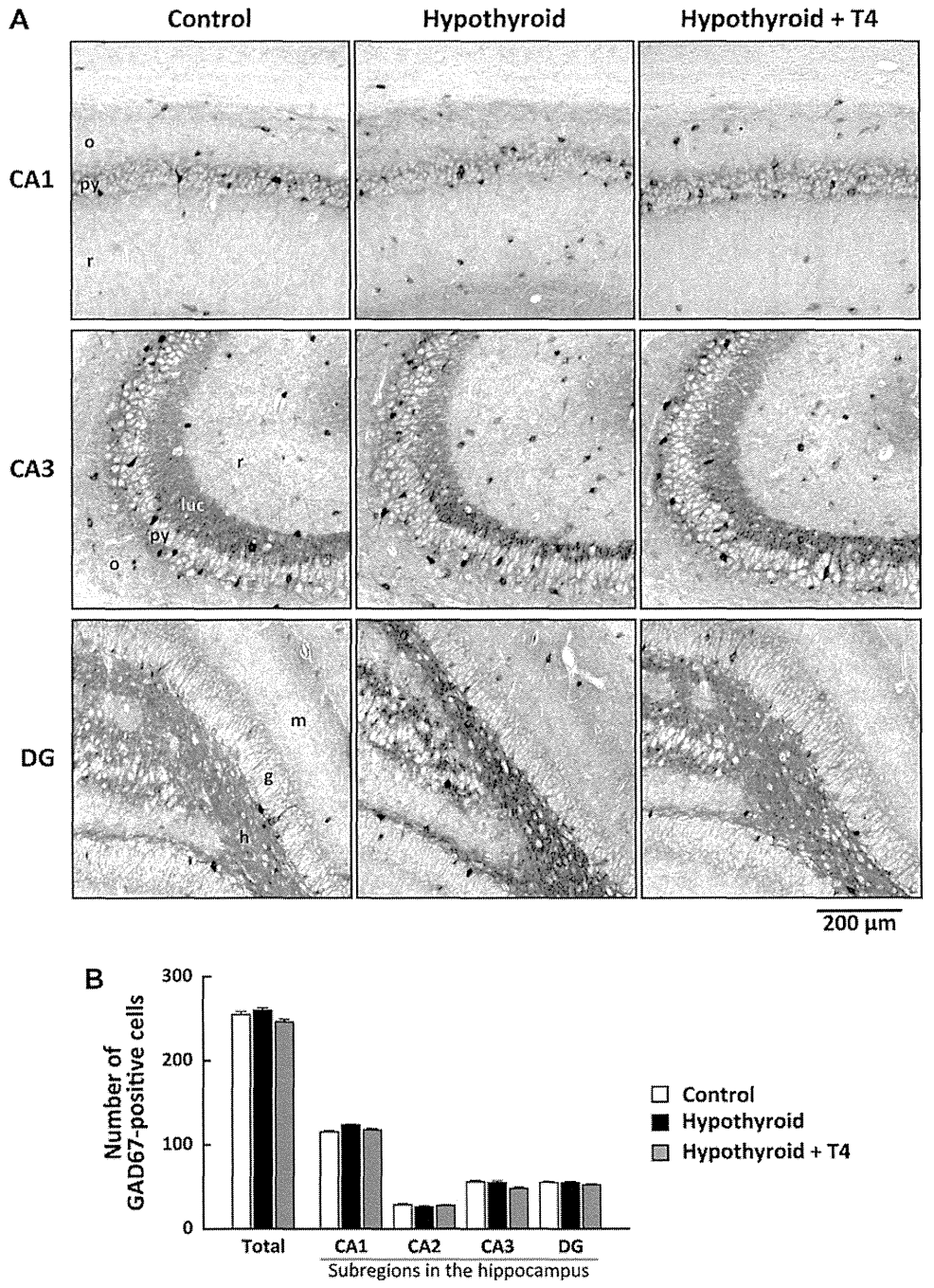

Fig. 4. Immunostaining with anti-GAD67 antibody in the hippocampus of control, hypothyroid and T4-replacement groups at PND28. Hippocampal sections (8 μm thick) from control, hypothyroid and T4-replacement groups at PND28 were stained with anti-GAD67 antibody. (A) Representataive photomicrographs of the hippocampal subregions (CA1, CA3 and DG) of control, hypothyroid and T4-replacement groups at PND28. (B) The number of GAD67-positive cells in the whole hippocampus and the hippocampal subregions (CA1, CA2, CA3 and DG) of control (open bar), hypothyroid (solid bar) and T4-replacement groups (shaded bar) were counted in each section obtained at PND28 and expressed as means + SEM. $n = 5–6$ (control, hypothyroid, T4-replacement groups). o: stratum oriens, py: stratum pyramidale, r: stratum radiatum, luc: stratum lucidum, m: stratum moleculare, g: stratum granulare, h: hilus. No significant difference in GAD67-positive cell number was observed between control and hypothyroid or hypothyroid and T4-replacement groups in any subregion.

were also observed in the postsynaptic components of the GABAergic system. Some of the GABA(A) receptor subunits (α1, γ2) showed up-regulation in the hypothyroid group and were normalized by T4-replacement at PND28 (Fig. 7A–C). Similar TH-responsive mRNA expression was observed with gephyrin, a scaffold protein localized to inhibitory synapses (Fig. 7D), but not in the guanine nucleotide exchange factor for CDC42, collybistin (*arhgef9*; Fig. 7E).

Another postsynaptic component strongly affected by TH status was the neuronal K^+/Cl^- co-transporter, KCC2, which is essential for the excitatory to inhibitory switching of the GABAergic neurotransmission (Fig. 8). In the control group, there was a strong transient up-regulation of *kcc2* at PND10, which was absent in the hypothyroid and the T4-replacement groups (Fig. 8A). Accordingly, KCC2 protein was reduced to 26% and 22% of control in the hypothyroid group at PND10 and PND15, respectively. Between PND15 and 28, however, there was a robust increase in KCC2 protein in the hippocampus of all 3 experimental groups including the hypothyroid group, so that it was comparable among these groups at PND28 (Fig. 8B).